A PRELIMINARY STUDY OF THE RESPONSE OF SINGLE ROTOR HELICOPTERS TO VORTEX ENCOUNTERS

by

H. C. Curtiss, Jr.
Zheng-gen Zhou

Department of Mechanical and Aerospace Engineering
Princeton University
Princeton, New Jersey

Report Number MAE 1699

Prepared For

U. S. Department of Transportation
Transportation System Center
Cambridge, Massachusetts

(Order No. DTRS57-84-P-81809)

April 1985

TABLE OF CONTENTS

	Page
SUMMARY	i
LIST OF FIGURES	iii
INTRODUCTION	1
DISCUSSION	3
VORTEX DISTURBANCE	5
Rotor Hub or Below Core ($\mathcal{Z}_H$ D 1)	12
Helicopter Response	21
Disturbance	21
Input to Helicopter	22
Vehicle Models	24
Response Calculations	24
CONCLUSIONS	29
RECOMMENDATIONS	30
REFERENCES	31
FIGURES	32
APPENDIX:	62
Flapping and Moment Characteristics of Helicopter Rotors	62
Mathematical Details	65
Table I	72
Figures	77

SUMMARY

The results of a preliminary study of the response of a single rotor helicopter to the gust field associated with the wing tip vortex of a large transport aircraft are presented. Consideration is given to the influence of rotor hub type (see-saw, articulated with offset, and hingeless) on the flapping and uncontrolled dynamic response of a helicopter to this gust field.

Estimates of the steady state flapping amplitude for a rotor located at various positions in the vortex field show that a lateral velocity component primarily produces a shift in phase of the flapping with little amplitude increase while the vertical velocity component produces a significant increase in flapping amplitude. It is shown that the effect of the gradient in vertical velocity on rotor flapping is not directly equivalent to roll rate of the helicopter shaft.

Predictions of the uncontrolled response of three example helicopters with different rotor types are presented based on linearized models. It is shown that the lateral velocity component of the vortex flow field produces a response primarily in the lateral/directional axes and the vertical component produces primarily a longitudinal response.

Only flight conditions in which the helicopters are inherently stable are examined and no feedback systems are considered with the exception of the Bell Bar which is an integral component of the UH-1H helicopter. This limits the flight conditions investigated to moderate forward speeds. The time responses in general are of large amplitude due to the magnitude of the vortex flow field which is characteristic of a Boeing 747. The amplitude of the response is smallest for the see-saw rotor helicopter and largest for the hingeless rotor

helicopter.

The primary term responsible for the response of a fixed wing aircraft to a vortex disturbance, the roll damping, is absent for the single rotor helicopter due to the different physical source of the roll damping for a helicopter.

LIST OF FIGURES

Figure		Page
1.	Main Rotor Types.	32
2.	Normalized Moment About Center of Gravity per Unit Flapping Angle.	32
3.	Influence of Hub Moment Parameters on Flapping Amplitude per Unit Control Deflection.	34
4.	Interpretation of Gust Gradients as Equivalent Motions of Aircraft.	35
5.	Vortex Flow Field.	36
6.	Blade Element Location in Flow Field.	37
7.	Spanwise Variation in Lateral Velocity Component.	38
8.	Velocity Components at Blade Element Induced by Vortex Flow Field.	39
9.	Typical Variation of Vertical Vortex Velocity with Blade Azimuth Angle at Constant Radial Location on Blade.	40
10.	Weighting Factors for Vertical Velocity Input to Rotor Flapping.	41
11.	Effect of a Lateral Velocity Disturbance on Rotor Blade Flapping.	42
12.	Steady State Flapping Induced by Vortex Flow Field. UH-1H Size Rotor (R_B = 3). Flapping Stiffness Varied.	43
13.	Steady State Flapping Induced by Vortex Flow Field. OH-6 Size Rotor (R_B = 1.6). Flapping Stiffness Varied.	44
14.	Disturbance Velocities for Dynamic Response Calculations.	45
15.	Helicopter Configurations.	46
16.	Characteristic Modes of Motion at 60 kts.	47
17.	UH-1H Lateral/Directional Response to Lateral Gust. V_o = 60 kts, W_{Rc} = 1200 fpm.	48
18.	UH-1H Lateral/Directional Response to Lateral Gust. Relative Velocity (Sideslip Velocity) Reponse.	49
19.	OH-5 Lateral/Directional Response to Lateral Gust. V_o = 60 kts, W_{Rc} = 1116 fpm.	50

20. BO-105 Lateral/Directional Response to Lateral Gust. 51
V_o = 60 kts, W_{Rc} = 1000 fpm.

21. UH-1H Lateral/Directional Response to Lateral Gust. 52
V_o = 100 kts, W_{Rc} = 1900 fpm.

Page

22. BO-105 Lateral/Directional Response to Lateral Gust. 53
V_o = 100 kts, W_{Rc} = 1000 fpm.

23. UH-1H Longitudinal Response to Vertical Gust (Aerodynamic Roll). 54
V_o = 60 kts, W_{Rc} = 1200 fpm.

24. UH-1H Longitudinal Response to Vertical Gust (Aerodynamic Roll). 55
V_o = 100 kts, W_{Rc} = 1900 fpm.

25. UH-1H Six Degree-of-Freedom Response to Lateral Velcoity Component of Vortex Flow Field. V_o = 60 kts, W_{Rc} = 1000 fpm. 56

26. UH-1H Six Degree-of-Freedom Resonse to Vertical Velocity Component of Vortex Flow Field. V_o = 60 kts, W_{Rc} = 1200 fpm. 58

27. Comparison of Predicted Response to Flight Test, UH-1H. 60
V_o = 60 kts, W_{Rc} 1200 fpm.

A-1. Shaft Angular Velocity Effects on Rotor Flapping. 76

A-2. Values of Integrals for Disturbance Evaluation. 77

A-3. Values of Integrals for Disturbance Evaluation. 78

Introduction

This report examines some aspects of the uncontrolled dynamic response of a single rotor helicopter to an encounter with the wing tip vortex of a large transport aircraft. The primary emphasis in the study was to investigate the importance of various design parameters of helicopters to the response characteristics.

Contemporary helicopters are equipped with three different types of main rotors: see-saw (Bell), fully articulated with hinge offset (Sikorsky, Hughes) and hingless (MBB, Westland, Aerospatiale) as illustrated in Figure 1. Flight test experiments have been conducted to investigate the response of a Bell UH-1 helicopter (see-saw rotor)[1,2] but there appears to be no experimental data related to other main rotor designs. Consequently, one of the questions of interest here is the influence of main rotor on the uncontrolled dynamic response of a single rotor helicopter to a vortex encounter. These three rotor types differ considerably in the magnitude of the moment about the center of gravity per unit of flapping angle as illustrated in Figure 2, while the magnitude of the flapping angle produced by a disturbance or control input is approximately independent of rotor type as shown in Figure 3 so it is expected that their response characteristics would differ. The relationships used to develop these figures are discussed in the Appendix. Shown on the figures are the values of the parameters for the three helicopters examined in this study.

This report describes the results of two analytical investigations. First the steady state increment in main rotor flapping induced by the vortex flow

field characteristic of a large transport aircraft (B-747) is examined. Experimentally measured data on the vortex characteristics are used to characterize this gust disturbance[3]. The results of this investigation are then used to determine the manner in which the vortex flow field would produce disturbance inputs on the entire helicopter. Time histories for the uncontrolled dynamic response of three helicopters are presented. The three example helicopters are the Bell UH-1H, Hughes OH-6A and the MBB BO-105C representing the three rotor types: see-saw; articulated with offset; and hingeless, respectively. Response calculations are based on linearized stability derivative models using the data presented in Reference 4.

Discussion

The response of an aircraft or helicopter to gust disturbances is estimated by assuming that the gust characteristics appear as relative velocities in the equations of motion. If the vehicle motion is described by a linearized model, then the effects of the gust disturbance on the vehicle appear through the aerodynamic stability derivatives. It is usually satisfactory to consider only the average value of the gust velocity at the vehicle and the gradient of the gust across the vehicle. A more detailed description of the gust field is not necessary if the problem of interest is to calculate the motion of the vehicle as a whole.

However, as pointed out in Reference 5, care must be taken in interpreting the effects of gradients in a gust field in estimating the forces and moments produced on a flight vehicle. There appears to be some confusion on this point in the literature. Reference 4 incorrectly describes how to include gust gradients in helicopter gust response calculations. While the constant or uniform parts of a gust field can be directly associated with aerodynamic forces exerted on an aircraft through changes in velocity, angle of attack and sideslip, interpretation of gust field gradients as angular velocities, depends in detail upon the physical sources contributing to the forces and moments on the aircraft. That is, as indicated in the sketch in Figure 4, for a fixed wing aircraft, while a gust gradient $\partial w/\partial y$, which will produce a spanwise variation in wing angle of attack, may be interpreted as an effective roll rate since the wing is the primary contributor to the roll damping (L_p), the gradient $\partial v/\partial z$ will have little effect on aerodynamic forces (there would be a small contribu-

tion from the spanwise angle of attack variation on the vertical tail) although both gradients would be encountered by a rolling aircraft. Therefore, first the flapping response of the main rotor of a helicopter to vertical and horizontal velocity gust gradients is examined, since it is this component of the helicopter that is sensitive to velocity gradients. The results of this investigation along with estimation of the contributions of the various components of a helicopter (main rotor, tail rotor, fuselage) to the stability derivatives are used to determine the input terms for the dynamic response simulation.

Vortex Disturbance

The flow field of the tip vortex used as the gust disturbance is based on experimental measurements from Reference 3 and is shown in Figure 5. An approximation to the velocity distribution given in Reference 3 is used to describe the tangential distribution of velocity of this vortex field. Reference 4 gives,

$$v_T = \frac{V_c(1+\ln \hat{r})}{\hat{r}} \qquad (\hat{r} > 0.8) \qquad (1)$$

where $\hat{r} = \frac{r}{r_c}$

The following functions also shown in Figure 5 are used to approximate the radial distribution given by equation (1),

$$\begin{aligned} v_T &= V_c \hat{r} && 0 < \hat{r} < 1 \\ v_T &= V_c(1.15 - .15\hat{r}) && 1 < \hat{r} < 3 \\ v_T &= V_c\,(.88 - .06\hat{r}) && 3 < \hat{r} < 10 \end{aligned} \qquad (2)$$

In the numerical studies, the experimental value of core radius, r_c and core velocity, V_c, are used:

$$r_c = 2.51\text{m}(8.23\text{ft})$$
$$V_c = 16\ \text{mps}(52.5\ \text{fps})$$

The vortex flow field is assumed to be two-dimensional, i.e., there is no variation of the velocity field in the x direction. It is convenient for the analysis that follows to resolve the tangential velocity into horizontal and vertical components of velocity v_v and w_v. As shown in Figure 5,

$$v_v = v_T \frac{\hat{z}}{\hat{r}}$$

$$w_v = -v_T \frac{\hat{y}}{\hat{r}}$$

The velocities have been expressed in terms of distances normalized by core radius.

To evaluate the effects of these velocity components on rotor blade motion the location of a blade element must be expessed in terms of blade azimuth angle ψ and blade element radial station from the hub, r_B. The only case considered here, which is expected to be the most critical one is with the rotor hub located on the vertical axis of the vortex. The vertical gust velocity has a gradient with zero average value. The horizontal gust has both an average value and a gradient in both the $\hat{y}$ and $\hat{z}$ directions. The effect of the gradient in the $\hat{y}$ direction is included. The effect of the $\hat{z}$ gradient on the helicopter is neglected. The hub is located a distance below the vortex centerline expressed in terms of core radii as $\hat{z}_H$ as shown in the Figure 6. Neglecting the small effect of blade flap angle on the location of the blade element, the coordinates of a blade element in the vortex flow field are as shown in Figure 6,

$$\hat{y} = \hat{r}_B \sin\psi$$
$$\hat{z} = \hat{z}_H$$

and the radial distance from the vortex center to the blade element is,

$$\hat{r} = \sqrt{\hat{z}_H^2 + \hat{y}^2} \qquad (3)$$

Thus, in general, the vertical and lateral velocity components experienced by a blade element located at $\hat{r}_B$, ψ are of the form

$$w_v = V_C \left\{ A \frac{\hat{r}_B \sin\psi}{\sqrt{\hat{z}_H^2 + \hat{r}_B^2 \sin^2\psi}} + B\, \hat{r}_B \sin\psi \right\}$$

$$v_v = V_c \left\{ A \frac{\hat{z}_H}{\sqrt{\hat{z}_H^2 + \hat{r}_B^2 \sin^2\psi}} + B\,\hat{z}_H \right\} \tag{4}$$

where A and B are constants that depend upon the location of the blade element and the hub. That is from equation (2)

$$\begin{aligned} 0 < \sqrt{\hat{z}_H^2 + \hat{r}_B^2 \sin^2\psi} < 1 \qquad & A = 0,\ B = 1 \\ 1 < \sqrt{\hat{z}_H^2 + \hat{r}_B^2 \sin^2\psi} < 3 \qquad & A = 1.15,\ B = -.15 \\ 3 < \sqrt{\hat{z}_H^2 + \hat{r}_B^2 \sin^2\psi} < 10 \qquad & A = 0.88,\ B = -.06 \end{aligned} \tag{5}$$

Note that if $\hat{z}_H \geq 1$ the blade element always remains outside the core, while when $\hat{z}_H$ is less than 1 each blade element passes in and out of the core as a function of $\hat{r}_B$ and aximuth angle depending upon whether

$$\sqrt{\hat{z}_H^2 + \hat{r}_B^2 \sin^2\psi}$$

is less than or greater than one. Two locations are considered in the analysis that follows $\hat{z}_H = 0$ and $\hat{z}_H \geq 1$. In the first case the rotor hub is located at the center of the vortex, there is no lateral velocity ($v_v = 0$) and the expression for vertical velocity becomes

$$w_v = - V_c \left\{ A \frac{\hat{r}_B \sin\psi}{|\hat{r}_B \sin\psi|} + B\,\hat{r}_B \sin\psi \right\} \tag{6}$$

Each blade element will pass in and out of the core as it rotates and a critical azimuth angle can be defined by

$$\sin\psi_{CR} = \frac{1}{\hat{r}_B} \tag{7}$$

If $\hat{r}_B$ is less than one, the blade element always remains inside the core and if $\hat{r}_B > 1$ equation (7) is used to determine the azimuth angle at which the blade passes out of the core. Equations (5) determine which of the three values of the constants should be used with equation (6) to determine the vertical velocity.

At $\hat{z}_H > 1$ there will be both vertical and lateral velocity components as given by equation (4) with the constants obtained from equation (5). It can be noted from equation (4) that v_v will have a spanwise variation across the rotor as shown in Figure 7. That is, at each edge of the rotor, the lateral velocity will be lower than at the centerline. As $\hat{z}_H$ increases this effect becomes weaker as shown in the figure. Now the effect of this velocity field on rotor blade flapping motion is determined.

Blade Flapping Motion

Figure 8 shows the added velocity components at a blade element. The additional velocity increments perpendicular and tangential to the blade section are

$$\Delta\bar{U}_p = \bar{w}_v - (\bar{v}_v \sin\psi)\,\beta$$
$$\Delta\bar{U}_T = -\bar{v}_v \cos\psi \qquad (8)$$

where the flapping angle β has been assumed small and the velocities have been normalized by the tip speed ΩR. The lift per unit span on the blade can be written as,

$$\ell = \frac{1}{2}\rho\, a\, c(\Omega R)^2 \left[\{x_B + \mu\sin\psi - \bar{v}_v\cos\psi\}^2\{\theta_o\}\right.$$
$$\left. - \{x_B + \mu\sin\psi - \bar{v}_v\cos\psi\}\{\lambda - (\mu\cos\psi + \bar{v}_v\sin\psi)\,\beta \right. \qquad (9)$$
$$\left. + \bar{w}_v - \beta' x_B\}\right]$$

The aerodynamic moment acting at the root of the blade is

$$M_\beta = R_B^2 \int_o^1 \ell\, x_B\, dx_B \tag{10}$$

From equations (9) and (10) the increment in aerodynamic flapping moment due to the velocity components v_v and w_v is

$$\begin{aligned}\Delta \frac{M_\beta}{I_B\Omega^2} = \frac{\gamma}{8} \{ & - \int_o^1 [8\, x_B\, \theta_o + 4\lambda]\, \bar{v}_v\, x_B\, dx_B \cos\psi \\ & - \int_o^1 4\, x_B^2\, \beta\, \bar{v}_v\, dx_B \sin\psi + \int_o^1 4\mu\beta\, \bar{v}_v\, x_B\, dx_B (\cos^2\psi - \sin^2\psi) \\ & + \int 4\beta'\, \bar{v}_v\, x_B^2 dx_B \cos\psi - \int_o^1 8\mu\theta_o\, \bar{v}_v\, x_B\, dx_B \sin\psi \cos\psi \\ & + \int_o^1 4\, \bar{v}_v^2\, \theta_o\, x_B\, dx_B \cos^2\psi + \int 4\bar{v}_v^2\, \beta\, x_B\, dx_B \cos\psi \sin\psi \\ & + \int_o^1 4\, \bar{v}_v\, \bar{w}_v\, x_B\, dx_B \cos\psi + \int_o^1 4\, \bar{w}_v\, x_B^2\, dx_B \\ & + \int_o^1 4\, \bar{w}_v\, \mu\, x_B\, dx_B \sin\psi \}\end{aligned} \tag{11}$$

In steady state conditions,

$$\beta = a_o - a_1 \cos\psi - b_1 \sin\psi$$

$$\beta' = a_1 \sin\psi - b_1 \cos\psi$$

The primary interest here is the steady state flapping and the overall response of the helicopter. Therefore, only the constant (a_o) and first harmonic flapping (a_1, b_1) increments are evaluated since these are the primary contributors to the vehicle response. The steady state flapping is of interest at different hub locations in the vortex since this will be a good indicator of the maximum flapping amplitudes to be expected in a vortex encounter. Two rotor hub locations are considered in some detail, first the rotor hub is located at

the vortex center ($\hat{z}_H = 0$), and second, the hub is located at or below the vortex core ($\hat{z}_H > 1$). These results are then faired smoothly between $\hat{z}_H = 0$ and $\hat{z}_H = 1$ to obtain suitable input fuctions for the time response calculations.

Case A: Rotor Hub at Vortex Center ($\hat{z}_H = 0$)

In this case the lateral gust velocity is zero and only two terms remain in the expression for ΔM_β. Equation (11) reduces to

$$\Delta \frac{M_\beta}{I_B \Omega^2} = \frac{\gamma}{8} \left\{ 4 \int_o^1 \bar{w}_v \, x_B^2 \, dx_B + 4\mu \int_o^1 \bar{w}_v \, x_B \, dx_B \sin\psi \right\} \qquad (12)$$

where for $\hat{z}_H = 0$

$$\bar{w}_v = \bar{V}_c \, \hat{f}_B \sin\psi \qquad \psi < \psi_{CR}$$

$$\bar{w}_v = \bar{V}_c \left(A \frac{\sin\psi}{|\sin\psi|} + B \, \hat{f}_B \sin\psi \right) \qquad \psi > \psi_{CR}$$

where $\hat{f}_B \sin\psi_{CR} = 1$ defines the critical azimuth angle. Now w_v is expanded in a Fourier Series with only the constant and first harmonic term retained

$$\bar{w}_v = \bar{w}_{vo} + \bar{w}_{vs} \sin\psi + \bar{w}_{vc} \cos\psi$$

It can be seen from the nature of the functions describing the dependence of w_v on azimuth angle that only sine terms exist and the constant and cosine terms are equal to zero. The typical variation of w_v with ψ is shown in Figure 9 for $\hat{f}_B > 1$. It can be seen by inspection that when $\hat{f}_B < 1$, such that the blade element always remains with the core

$$\bar{w}_{vs} = \bar{V}_c \, \hat{f}_B$$

When $\hat{f}_B > 1$, the Fourier coefficient must be calculated. The development is given in the Appendix. In general w_{vs} can be expressed as

$$\bar{w}_{vs} = \bar{V}_c \, g(\hat{r}_B)$$

where the function $g(\hat{r}_B)$ is shown graphically in Figure 10. Denote

$$F_w(\hat{R}_B) = \frac{4}{\hat{R}_B^4} \left(\int_o^1 \hat{r}_B^3 \, d\hat{r}_B + \int_1^{\hat{R}_B} g(\hat{r}_B) \, \hat{r}_B^2 \, d\hat{r}_B \right) \tag{13}$$

The first term accounts for the blade section within the core and the second term, the blade section that passes in and out of the core. The first term in equation (12) becomes

$$\frac{\gamma}{8} \bar{V}_c \, \hat{R}_B F_w(\hat{R}_B) \sin\psi \tag{14}$$

The second term in equation (12) involves one less power of x_B and also involves the sine of the azimuth angle and thus will produce a constant and second harmonic term. The second harmonic is neglected as it will not produce motion of the helicopter on a whole. Denote

$$G_w(\hat{R}_B) = \frac{3}{\hat{R}_B^3} \left(\int_o^1 \hat{r}_B^2 \, d\hat{r}_B + \int_1^{\hat{R}_B} g(\hat{r}_B) \, \hat{r}_B \, d\hat{r}_B \right) \tag{15}$$

and noting that

$$\frac{1}{2\pi} \int_o^{2\pi} \sin^2\psi \, d\psi = \frac{1}{2}$$

the second term becomes

$$\frac{\gamma}{8} \frac{2}{3} \mu \, \bar{V}_c \, \hat{R}_B \, G_w(\hat{R}_B) \tag{16}$$

Thus there is a $\sin\psi$ disturbance produced by the first term in equation (12) given by equation (14) and a second term which is a constant given by equation (16). The constant term will provide a change in the coning angle and the $\sin\psi$ term will produce a $\cos\psi$ or fore and aft flapping on an articulated rotor. The

constant term will also produce a change in thrust. Figure 10 also shows $F_w(R_B)$ and $G_w(R_B)$ over the range of interest ($R_B < 3$) indicating that for the size of the helicopters under consideration here,

$$G_w(\hat{R}_B) \approx F_w(\hat{R}_B)$$

Consequently, it is possible to interpret the influence of the vertical velocity distribution as equivalent to an effective aerodynamic roll rate. Comparison with the conventional flapping equation given in the Appendix shows that,

$$P_{Ae} = \Omega \bar{V}_c \hat{R}_B \, F_w(\hat{R}_B) = \frac{V_c}{r_c} F_w(\hat{R}_B) \tag{17}$$

The effective roll rate depends only upon the vortex characteristics and the size of the rotor relative to the core of the vortex. Summing the two effects in equations (14) and (16) and using the definition in equation (17)

$$\Delta \left(\frac{M_\beta}{I_B \Omega^2}\right) = \frac{\gamma}{8} \left(\frac{2}{3}\mu + \sin\psi\right) \frac{P_{Ae}}{\Omega} \tag{18}$$

Thus the size of the flapping disturbance produced by vertical velocity depends on the ratio of the effective aerodynamic roll rate to the rotor angular velocity. The significance of this result for various size helicopters is discussed later in the report.

Rotor Hub or Below Core ($\hat{z}_H \geq 1$)

At this location of the rotor hub, the blade elements are always outside the vortex core. Thus the expressions for the vertical and horizontal velocity components are

$$w_v = V_c \left(A \frac{\hat{r}_B \sin\psi}{\sqrt{\hat{z}_H^2 + \hat{r}_B^2 \sin^2\psi}} + B \hat{r}_B \sin\psi\right)$$

$$v_v = V_c \left(A \frac{\hat{z}_H}{\sqrt{\hat{z}_H^2 + \hat{r}_B^2 \sin^2\psi}} + B\, \hat{z}_H \right) \tag{4}$$

A and B are constants depending upon the location of the blade element. Again only the constant and first harmonic contributions to the aerodynamic flapping moment are calculated. It can be seen from equation (11) that the following integrals are needed in the process of determining the contributions of the gust velocity components to the constant and first harmonic flapping moments.

$$F_{NsMc} = \frac{1}{\pi} \int_o^{2\pi} \frac{\sin^N\psi \cos^M\psi \, d\psi}{\sqrt{\hat{z}_H^2 + \hat{r}_B^2 \sin^2\psi}}$$

$$F^*_{NsMc} = \frac{1}{\pi} \int_o^{2\pi} \frac{\sin^N\psi \cos^M\psi \, d\psi}{\hat{z}_H^2 + \hat{r}_B^2 \sin^2\psi}$$

Evaluation of these intergrals is given in the Appendix. The first set of integrals are elliptic and can be evaluated using standard tables. The numerical values of these integrals are presented in Figures A-2 and A-3 in the Appendix. Denote

$$I^{\ell}_{NsMc} = \frac{\ell}{\hat{R}_B^{\ell}} \int_o^{\hat{R}_B} [A\, F_{NsMc} + k^*_{NsMc}\, B]\, \hat{r}_B^{\ell-1}\, d\hat{r}_B$$

This integral has the following limit values. For: B = 1, A = 0,

$$I^{\ell}_{NsMc} \rightarrow k^*_{NsMc}$$

For a vanishingly small rotor ($r_B \rightarrow 0$) or equivalently the value of the integrals at the rotor hub for $\hat{z}_H > 1$,

$$F_{NsMc} \rightarrow \frac{k^*_{NsMc}}{\hat{z}_H}$$

$$F^*_{NsMc} \rightarrow \frac{k^*_{NsMc}}{\hat{z}_H^2}$$

Thus, the integrals which appear in the flapping moment equations (I_{NsMc}, I^*_{NsMc}) multiplied by $\hat{z}_H$, are the sideslip or lateral velocity effects averaged across the rotor. In the limit as the rotor becomes vanishingly small ($R_B \rightarrow 0$), these integrals become

$$I^{\ell}_{NsMc} \rightarrow k^* \left[\frac{A}{\hat{z}_H} + B\right]$$

where $\bar{V}_c\left(\frac{A}{\hat{z}_H} + B\right)$ is the value of the lateral velocity on the vertical axis, normalized by tip speed.

The increment in flapping moment written in terms of these integrals is

$$\begin{aligned}
\Delta \frac{M_B}{I_B \Omega^2} = \frac{\gamma}{8} \{ & [\bar{V}_c \hat{z}_H \{ -\frac{8}{3}\theta_o I^3_{2c} - 2\lambda I^2_{2c} - 2\mu a_1 (I^2_{4c} - I^2_{2c2s})\} \\
& - 2\bar{V}_c^2 \hat{z}_H^2 b_1 I^{*2}_{2c2s}] \cos\psi \\
& + [\bar{V}_c \hat{z}_H \{ -\frac{4}{3} a_o I^3_{2s} - 2\mu b_1 (I^2_{2c2s} - I^2_{4s})\} \\
& - 2\bar{V}_c \hat{z}_H^2 a_1 I^{*2}_{2c2s} + \underline{\bar{V}_c \hat{R}_B I^4_{2s}}] \sin\psi \\
& + \bar{V}_c \hat{z}_H \{\mu_x a_o [I^2_{2c} - I^2_{2s}] - \frac{2}{3} b_1 [I^3_{2c} - I^3_{2s}]\} \\
& + \bar{V}_c^2 \hat{z}_H^2 \theta_o I^{*2}_{2c} + \underline{\frac{2}{3} \mu_x \bar{V}_c \hat{R}_B I^3_{2s}} \}
\end{aligned} \tag{19}$$

The underlined terms are due to the vertical velocity component, w_v, while the remaining terms are due to the lateral velocity component, v_v. When $\hat{z}_H = 0$,

$$I^4_{2s}(\hat{z}_H, \hat{R}_B) \to F_w(\hat{R}_B)$$

$$I^3_{2s}(\hat{z}_H, \hat{R}_B) \to G_w(\hat{R}_B) \cong F_w(\hat{R}_B)$$

and consequently equation (19) reduces to equation (18) for the case when the rotor hub is located at the vortex center. For a vanishingly small rotor located at $\hat{z}_H = 1$, the equation (19) reduces to

$$\Delta\left(\frac{M_\beta}{I_B\Omega^2}\right)_{\hat{R}_B \to o} = \frac{\gamma}{8}\left\{\left[\mu_y\left\{-\frac{8}{3}\theta_o - 2\lambda - \mu_x a_1\right\} - \frac{1}{2}\mu_y^2 b_1\right]\cos\psi\right.$$

$$+ \left[\mu_y\left\{-\frac{4}{3}a_o + \mu_x b_1 - \frac{\mu_y^2}{2}a_1\right\} + \bar{P}_{Ae}\right]\sin\psi \qquad (20)$$

$$\left. + \mu_y^2\theta_o + \frac{2}{3}\mu_x\bar{P}_{Ae}\right\}$$

where $\bar{P}_{Ae}$ is the normalized effective aerodynamic roll rate

$$\bar{P}_{Ae} \to \bar{V}_C \hat{R}_B = \frac{V_C}{\Omega r_C}$$

and μ_y is the normalized sideslip disturbance, i.e., sideslip advance ratio, while μ_x is the flight advance ratio before the disturbance is encountered, i.e., the resultant advance ratio of the rotor after encountering the disturbance is

$$\mu_R = \sqrt{\mu_x^2 + \mu_y^2}$$

Equation (20) differs from the standard development of the rotor flapping moment equation as found for example in Reference 6 where a wind axis system is used, so that the effect of a lateral velocity disturbance (μ_y) appears as an

increase in resultant advance ratio and a shift in phase of the flapping because the azimuth reference is downwind and this varies with lateral velocity.

Expressions for the flapping coefficients can be obtained from the balance of aerodynamic and inertial moments about the flapping hinge. The hingeless rotor is modelled by a spring on the flapping hinge which introduces the ratio of flap frequency to rotor angular velocity p into the flapping equation, (see Appendix). The equation of motion for blade flapping, β, obtained by summing moments about the flapping hinge is,

$$\beta'' + \frac{\gamma}{8}(1 + \frac{4}{3}\mu_x \sin\psi)\,\beta' + (p^2 + \frac{\gamma\mu_x}{8}\cos\psi + \frac{\gamma\mu_x^2}{8}\sin 2\psi)\,\beta$$
$$= \frac{\gamma}{8}\left[\frac{8}{3}\theta_o\mu_x + 2\lambda\mu_x\right]\sin\psi + \Delta\left[\frac{M_\beta}{I_B\Omega^2}\right] \qquad (21)$$

Introducing the expression for ΔM_β from equation (19), then the method of harmonic balance is used to obtain expressions for the constant and first harmonic flapping terms, where for steady state flapping motion,

$$\beta = a_o - a_1\cos\psi - b_1\sin\psi$$
$$\beta' = a_1\sin\psi - b_1\cos\psi$$
$$\beta'' = a_1\cos\psi + b_1\sin\psi$$

Thus the equations for coning and flapping are

$$a_o = \frac{\gamma}{8p^2}\left[\theta_o(1 + \mu_x^2 + \underline{\bar{V}_c^2\,\hat{z}_H^2\,I_{2c}^{*2}}) + \frac{4}{3}\lambda\right.$$
$$+ \bar{V}_c\hat{z}_H\{\mu_x a_o\,\underline{[I_{2c}^2 - I_{2s}^2]} - \frac{2}{3}b_1\,[I_{2c}^3 - I_{2s}^3]\}$$
$$\left. + \underline{\frac{2}{3}\mu_x\,[\bar{V}_c\,\hat{R}_B I_{2s}^3]}\right] \qquad (22)$$

$$\left[\frac{8}{\gamma}(1 - p^2) + \underline{\bar{V}_c \hat{z}_H 2\mu_x (I^2_{2c2s} - I^2_{4s})}\right] b_1$$

$$+ \left[1 - \frac{\mu_x^2}{2} + \underline{2\bar{V}_c^2 \hat{z}_H^2 I^{*2}_{2c2s}}\right] a_1$$

$$= \left[\frac{8}{3}\theta_o + 2\lambda\right]\mu_x - \underline{\bar{V}_c \hat{z}_H \left[\frac{4}{3} a_o I^3_{2s}\right]}$$

$$+ \underline{\underline{\bar{V}_c \hat{R}_B I^4_{2s}}}$$

$$\left[-\frac{8}{\gamma}(1 - p^2) - \underline{\bar{V}_c \hat{z}_H 2\mu_x (I^2_{2c2s} - I^2_{4s})}\right] a_1 + \left[1 + \frac{\mu_x^2}{2} - \underline{2\bar{V}_c^2 \hat{z}_H^2 I^{*2}_{2c2s}}\right] b_1$$

$$= \frac{4}{3} a_o \mu_x + \underline{\bar{V}_c \hat{z}_H \left[\frac{8}{3}\theta_o I^3_{2c} + 2\lambda I^2_{2c}\right]}$$

Single underlined terms are the effects of lateral velocity and double underlined terms are the effect of vertical velocity.

First consider the effects of lateral velocity on steady state flapping. The lateral velocity effects are largest when $\hat{z}_H = 1$ and are proportional to V_c times various integrals. These integrals are always less than their corresponding limiting values for a vanishingly small rotor (k^*_{NcMs}) due to averaging across the rotor disc. In this limit case, the physical nature of these effects is as follows. The advance ratio is increased from the flight advance ratio μ_x to $\sqrt{\mu_x^2 + V_c^2}$. The largest change in advance ratio occurs near hover. For tip speeds characteristic of modern helicopters ($\Omega R \cong 700$ fps),

$$\bar{V}_c \cong .075$$

At an advance ratio $\mu_x = .15$ (≈ 60 kts) the change in resultant advance ratio due to the core velocity is

$$\Delta\mu_R = \sqrt{\mu_x^2 + \bar{v}_c^2} - \mu_x = .018$$

Thus there is only a small increase in advance ratio due to vortex core velocity in translational flight. Due to the symmetric nature of the rotor, the flapping will shift in phase by an amount

$$\beta = \tan^{-1} \frac{.075}{.15} = 26.6°$$

The phase shift will produce the primary effect on the helicopter and there will be little change in amplitude of the flapping due to the small change in resultant advance ratio. The physical picture is sketched in Figure 11. The moment produced on the helicopter by the change in flapping due to lateral velocity will be primarily a result of the phase shift in flapping causing a rolling moment perturbation on the helicopter. This is the physical source of the dihedral effect of a helicopter arising from the main rotor. Including the lateral velocity distribution will reduce the size of this effect and will make the interpretation less straightforward since the various integrals in equations (22) have different values. The averaging associated with a sine disturbance is different from a cosine effect.

The vertical velocity disturbance is considerably more significant in inducing flapping motion. It has been noted that the vertical velocity gradient is similar to an aerodynamic roll rate. That is, comparison of the new flapping equations (22) with those given in the Appendix including the rotor shaft pitch and roll rate taken from Reference 7 shows that aerodynamic roll is not equivalent to a rolling velocity of the shaft. A shaft roll velocity (P_s) produces the following flapping increments on an articulated rotor

$$\Delta a_0 = \frac{\gamma}{6} \mu P_s$$

$$\Delta a_1 = -\frac{P_s}{\Omega} \qquad (23)$$

$$\Delta b_1 = -\frac{16}{\gamma\Omega} P_s$$

From the equation (22) with $\hat{z}_H = 0$ for an articulated rotor (p = 1),

$$\Delta a_o = \frac{\gamma}{6}(\mu \bar{V}_c \hat{R}_B I_{2s}^3)$$

$$\Delta a_1 = \bar{V}_c \hat{R}_B I_{2s}^4$$

$$\Delta b_1 = 0$$

Lateral tilt of the rotor plane (Δb_1) is not produced by the vertical velocity gradient. This is because the lateral tilt (Δb_1) given in equation (23) is an inertial response which can be seen by the appearance of the Lock Number, γ, which is equal to,

$$\gamma = \frac{\rho a c R^4}{I_B}$$

The lateral flapping produced by shaft roll rate is proportional to the blade flapping moment of inertia demonstrating that the source of this term is inertial.

Thus the vertical velocity disturbance produces only a change in coning and longitudinal flapping on an articulated rotor. For an articulated rotor helicopter, this will primarily result in a longitudinal response. For a hingeless rotor, phase shift will produce some roll disturbance as well.

Calculations of the increment in steady state flapping produced by the vor-

tex field are shown in Figures 12 and 13 for two different size helicopter rotors at two advance ratios at $\hat{z}_H = 0$ and $\hat{z}_H = 1$. The effect of varying the flapping stiffness is also shown. It can be noted that the primary change occurs in longitudinal flapping and is due to the vertical velocity gradient. The flapping stiffness (p) has little effect on the magnitude of the flapping and primarily produces a shift in phase of the flapping. The magnitude of the flapping increase is about the same for both size rotors even though one rotor is considerably larger than the other. The increase is about the same because of the fact that most helicopters have similar tip speeds, so that there is a tradeoff between the weighting factor due to rotor size ($F_w(R_B)$) and rotor RPM. That is, at $\hat{z}_H = 0$ for example,

$$\Delta a_1 = \bar{V}_c \hat{R}_B F_w(\hat{R}_B)$$

$$= \frac{V_c}{\Omega r_c} F_w(\hat{R}_B)$$

V_c and r_c are vortex characteristics. As the rotor radius increases compared to the vortex, the factor $F_w(R_B)$ decreases, but since the tip speed is constant, Ω decreases and the ratio of F_w to Ω remains about the same. Thus to the first order, the longitudinal flapping amplitude is about the same for different size helicopters. For the two helicopter rotors used in the example,

(OH-6) $\hat{R}_B = 1.6$, $\Omega = 470$ RPM, $F(\hat{R}_B) = 0.8$

(UH-1H) $\hat{R}_B = 3.0$, $\Omega = 320$ RPM, $F(\hat{R}_B) = 0.46$

Thus

$$\Delta a_1 \sim \frac{F(\hat{R}_B)}{\Omega} \sim 17 \times 10^{-4} \quad \text{(OH-6)}$$

$\sim 14 \times 10^{-4}$ (UH-1H)

It can also be noted by observing that the flapping amplitude increase at $\hat{z}_H = 1$ is about the same as at $\hat{z}_H = 0$ (no lateral velocity) that the lateral velocity disturbance produces only a small increase in flapping amplitude for reasons described above. The largest flapping amplitude increase due to a lateral velocity disturbance would occur when the helicopter encountered the vortex while hovering since then the lateral velocity increase would correspond directly to a change in advance ratio.

Helicopter Response

In this section, the uncontrolled dynamic response of single rotor helicopters to a vortex encounter is examined and time histories presented for three helicopters representing each of the three rotor types.

Disturbance

Based on the previous discussion, the equivalent vertical and lateral velocity disturbance velocities produced by the vortex can be represented as shown in Figure 14. The lateral velocity or sideslip disturbance appears as one cycle of a sawtooth wave and the vertical velocity gradient disturbance is triangular in shape. The disturbance velocities have been faired to zero at ten core radii from the vortex center. Other assumptions regarding the spatial variation of the disturbance velocities at initial encounter had little effect on the response. The time scale of the disturbance is determined by the vertical climb rate of the helicopter.

The maximum equivalent vertical velocity gradient is determined by the effective aerodynamic roll rate calculated by the method presented in the pre-

vious section. The maximum sideslip velocity is taken as the value on the vortex centerline and the averaging discussed in the previous section for the main rotor is not used as the effect is not large and occurs only on the main rotor and not the tail rotor. This should give a somewhat conservative result for the magnitude of the response to the lateral velocity.

Input to Helicopter

In general, the lateral and longitudinal dynamics of a helicopter are coupled and inputs will appear in all six equations of motion. Considering the six force and moment equations, the following stability derivatives exist related to lateral velocity and roll rate

$$X_v,\ Y_v,\ Z_v,\ L_v,\ M_v,\ N_v$$

$$X_p,\ Y_p,\ Z_p,\ L_p,\ M_p,\ N_p$$

In accordance with the previous discussion to determine which of these derivatives should be included in the input terms, the physical source of the derivatives must be identified. In the case of the lateral velocity derivatives, they are all aerodynamic in nature and thus the input is of the form

$$\text{X-FORCE} = -X_v v_v$$

$$\text{Y-FORCE} = -Y_v v_v$$

$$\text{Z-FORCE} = -Z_v v_v$$

$$\text{Roll Moment} = -L_v v_v$$

$$\text{Pitch Moment} = -M_v v_v$$

$$\text{Yaw Moment} = -N_v v_v$$

In general, the large terms tend to be those associated with lateral-directional equations, i.e.,

$$-Y_v v_v,\ -L_v v_v;\ -N_v v_v$$

and the effects on the longitudinal motion do not appear large. Some comparisons were made between the three degree-of-freedom lateral/directional response and the complete six degree-of-freedom response including all terms which showed that the response to the lateral velocity disturbance is primarily lateral/directional for the particular helicopter investigated. Some helicopters may have significant values of pitching moment due to lateral velocity (M_v) produced by rotor wake interaction with the horizontal tail which could lead to an increased pitch response[8]. For the vertical velocity gradient, input terms appear as an effective aerodynamic roll rate, consequently, the roll rate derivatives which arise from inertial effects must be identified. As discussed in the previous section, a shaft rolling velocity produces on an articulated rotor longitudinal flapping due to aerodynamic effects and lateral flapping due to inertial effects. The derivatives Y_p and L_p are primarily determined by the main rotor lateral flapping due to roll rate and thus these derivatives are set equal to zero for the vertical velocity gradient input. Thus, the stability derivative that is primarily responsible for the response of a fixed wing aircraft to a vortex encounter, L_p, is absent in the disturbance input for a helicopter. Consequently, the response of a helicopter to a vertical velocity gradient will occur primarily in the longitudinal axis as the only remaining lateral/directional input, N_p, tends to be small. This is shown later by comparing the three degree-of-freedom longitudinal response to the complete six

degree-of-freedom response with N_p included as an input term.

Vehicle Models

The helicopters are modelled using linearized equations of motion in a conventional Eulerian reference frame. It is important to note that in the time histories presented, the perturbation velocities are with respect to a body axis reference frame. The values of the derivatives are taken from Reference 4 for the three helicopters investigated. While the calculations indicate large amplitude motions, indicating that non-linear effects maybe present it is considered that the simpler linear model should be reasonably representative of the response and also is better able to promote physical insight into the features of the response. Three helicopters are investigated: a Bell UH-1H (see-saw rotor); a Hughes OH-6A (articulated rotor with offset), MBB BO-105 (hingeless rotor). Side views are shown in Figure 15. The physical parameters and stability derivatives of the three vehicles are given in Table I, obtained from Reference 4. The UH-1H model includes the feedback provided by the stabilizer bar.

Response Calculations

Various time histories of the uncontrolled response of the three helicopters to a vortex encounter are presented and discussed in this section. One of the problems associated with investigating the uncontrolled response of helicopters is that in many flight conditions they are marginally stable or unstable (without automatic stabilization) and the calculation of the uncontrolled response results in very large amplitude motions which are not of practical interest. This tends to be the situation for both the longitudinal and lateral/directional characteristics near hover and the longitudinal motions in

translational flight. The lateral/directional characteristics of the example helicopters at a translational velocity of 60 kts are stable as indicated by the characteristic roots shown in Figure 16. Also shown are the longitudinal characteristics. The hingeless rotor helicopter (BO-105) is unstable and the Oh-6 is marginally stable in translational flight while the UH-1H is stable. Therefore no calculations of the longitudinal motions of the OH-6 and BO 105 are shown. As the flight velocity is reduced the lateral/directional motions tend to become unstable as well. Thus calculations are presented for 60 and 100 kts trim velocities only. To extend these investigations to low speeds it would be necessary to add automatic stabilization or to model a pilot-in-the loop using a relatively simple feedback model. In this way it is possible to gain insight in cases where the inherent stability of a helicopter is poor.

Figures 17-21 present the results of time history calculations based on the stability derivatives and vehicle physical parameters of Reference 4. Consider first the three-degree-of-freedom lateral response to the lateral gust component of the vortex flow field for the UH-1H at 60 kts shown in Figure 17. Lateral velocity, roll angle and yaw rate time histories are shown. The lateral gust velocity is also shown and the sideslip of the vehicle is proportional to the difference between these two curves. The lateral velocity response of the vehicle has a shape similar to the input or gust velocity with a time lag due to the inertia and other aerodynamic characteristic of the vehicle. Essentially if the vehicle had no mass, the lateral velocity of the vehicle would tend to be equal to the disturbance velocity. Since the difference between these two curves is the sideslip velocity of the vehicle relative to the air, this velocity difference can be considered as the "input" to the rolling and yawing moment

equations. That is, if $v = v_v$ there would be little rolling or yawing motion. Figure 18 shows the relative or sideslip velocity and comparison with Figure 17 shows that the roll and yaw motions are primarily produced by this velocity.

Figures 19 and 20 show the lateral/directional response to a lateral gust input for the BO-105 and OH-6 at 60 knots. These responses are quite similar to the UH-1H response due to the similarity in dutch roll characteristics of the three helicopters. The peak roll angle experienced by the OH-6A and the BO-105 are larger than the UH-1H due primarily to the larger dihedral effect associated with hinge offset for the OH-6 and the hingeless rotor in the case of the BO-105. The maximum roll angle experienced by the UH-1H is about 10°, the OH-6 about 20°; and about 30° on the BO-105. The values of the dihedral effect are:

UH-1H	$L'_v = -.0133$
OH-6A	$L'_v = -.0567$
BO-105	$L'_v = -.0803$

The amplitude increase with rotor type is not directly proportional to dihedral effect due to the fact that the roll damping increases as well tending to counter the gust induced roll motion. The roll damping for the three helicopters are:

UH-1H	$L'_p = -.799$
OH-6A	$L'_p = -4.97$
BO-105	$L'_p = -9.17$

The yaw rate response is quite similar for the UH-1H and BO-105. The OH-6 exhibits a considerably larger yaw rate response due to its larger directional sta-

bility. The directional stability characteristics of single rotor helicopters are largely not a function of main rotor type as the primary contributors to the directional stability are the tail rotor, fixed vertical tail surfaces and the fuselage. Figures 21 and 22 show lateral/directional responses at 100 kts indicating only a weak effect at higher speeds. At higher airspeeds than examined here there is a tendency for the dutch roll to exhibit less damping perhaps becoming a more critical case.

The three-degree-of-freedom pitching response of the UH-1H is shown in Figures 23 and 24 for trim speeds of 60 and 100 kts. The amplitude of the response is large especially at 60 kts although somewhat smoother and perhaps more easily countered by the pilot than the lateral/directional response. This is of course to a large extent due to the nature of the input disturbance shown in Figure 14. There is quite a strong effect of airspeed on the uncountrolled pitch response of the UH-1H, the maximum pitch angle reducing by about a factor of two as the airspeed is increased from 60 kts to 100 kts due to the improving longitudinal stability with airspeed. Figure 25 shows a six-degree-of-freedom response of the UH-1H with all coupling terms to the lateral gust component. Very little longitudinal motion occurs and the lateral/directional response is essentially the same as the three-degree-of-freedom response in Figure 17. Figure 26 shows the six-degree-of-freedom response to the vertical velocity for the UH-1H. While the longitudinal motion is unchanged from Figure 25 there also is some lateral/directional motion due apparently to the yawing moment due to roll rate as well as other coupling terms in the equation of motion. The maximum roll amplitude is similar to that from the lateral velocity input. This response however may be somewhat unrealistic due to the large amplitude of the

longitudinal motion. That is, as indicated above, the sideslip or lateral velocity input primarily produces a lateral/directional response and the vertical velocity gradient or effective aerodynamic roll rate primarily produces a longitudinal response.

It may be noted in general from these results that the longitudinal response is quite smooth and probably somewhat easier for the pilot to control then the lateral/directional response which exhibits considerably more of an oscillatory character largely due to the nature of the input as well as the fact that the typical dutch roll motion of a helicopter is relatively lightly damped and of reasonably high frequency.

Figure 26 shows a comparison of the calculated response for the UH-1H with flight test results presented in Reference 1. It should be noted that in the flight test the aircraft generating the tip vortex was considerably smaller than a B-747. It can be seen that the general shape of the response is quite satisfactorily predicted by the approach presented in this report.

Conclusions

1.) One primary source of the response of a fixed wing aircraft to a vortex flow field, the roll damping does not appear as an input term for a single rotor helicopter. Helicopter roll rate is not completely equivalent to a vertical velocity gradient.

2.) The vortex vertical velocity distribution primarily produces a response of the helicopter in the longitudinal axes.

3.) The lateral velocity distribution in the vortex pimarily produces a lateral/directional response.

4.) The general character of lateral/directional response of the different type single rotor helicopter examined was similar. The magnitude of the response was largest for the hingeless helicopter and smallest for the see-saw rotor.

5.) The primary contribution to flapping amplitude is the vertical velocity distribution. The amplitude of the flapping induced is reasonably large and relatively insensitive to rotor diameter.

6.) It was not practical to examine the longitudinal response of the articulated and hingeless rotor helicopters due to their lack of inherent stability.

Recommendations

1.) To expand the range of the flight conditions, it would be desirable to incorporate a simple feedback model for a pilot to provide inherent stability such that the complete speed range could be examined. This approach should promote insight into the helicopter response in other flight conditions.

2.) The general nature of the results of this study indicate that it would be highly desirable to conduct studies of the helicopter response using a flight simulator in order to evaluate the ability of a pilot to minimize the response of a helicopter in a vortex encounter. The lightly damped short period dutch roll mode characteristic of a helicopter and the nature of the lateral velocity disturbance may make it difficult for the pilot to reduce the rolling motion induced by the vortex.

3.) The magnitude of the tail rotor flapping induced by the disturbance should be investigated.

References

1. Dunham, R. E., Mantay, W. R., Campbell, R. L.,and Van Gunst, R. W.: Flight-Test Experience of a Helicopter Encountering an Airplane Trailing Vortex, AHS Annual Forum, 1976, Preprint 1063.

2. Mantay, W. R., Holbrook, G. T., Campbell, R. L. and Tomaine, R. L.: Flight Investigation of the Response of a Helicopter to the Trailing Vortex of a Fixed Wing Aircraft.

3. Burham, D. C.: B-747 Vortex Alleviation Flight Tests: Ground Based Sensor Measurements, DOT-FAA-RD-81-99, February 1982.

4. Heffley, R. K., et al: A Compilation and Analysis of Helicopter Handling Qualities Data, NASA Contractor Report 3144, August 1979.

5. McRuer, D., Ashkenas, I., and Graham, D.: "Aircraft Dynamics and Automatic Control," Princeton University Press, Princeton, NJ 1973.

6. Gessow, A. and Myers, A. C.: "Aerodynamics of the Helicopter," F. Ungar, New York, NY.

7. Seckel, E., and Curtiss, H. C.: Aerodynamic Characteristics of Helicopter Rotors, Princeton University, Department of Mechanical and Aerospace Engineering Report, 659, December 1963.

8. Cooper, D. E.: YUH-60A Stability and Control, AHS Annual Forum, 1977, Preprint 77-33-29-4000.

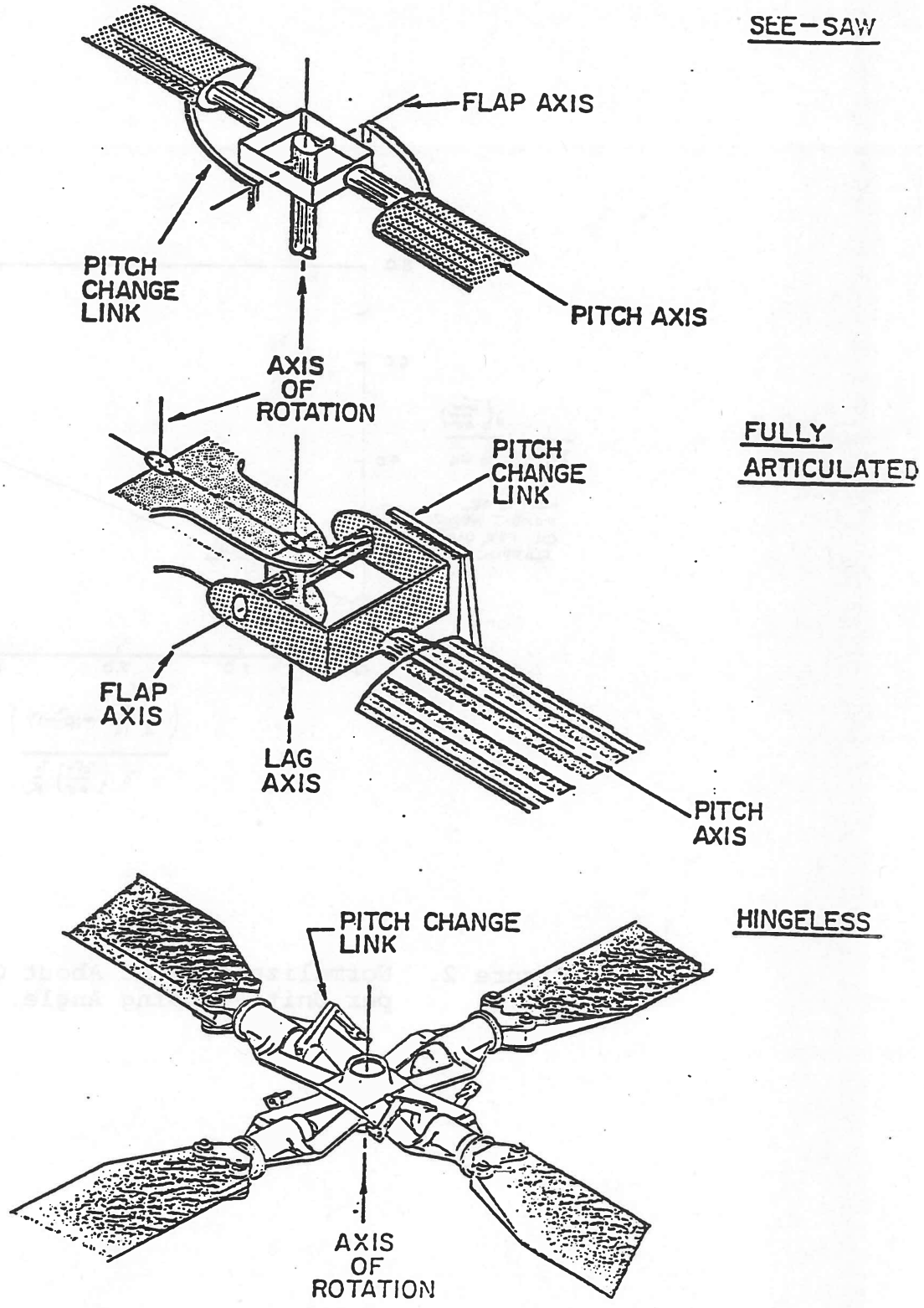

Figure 1. Main Rotor Types.

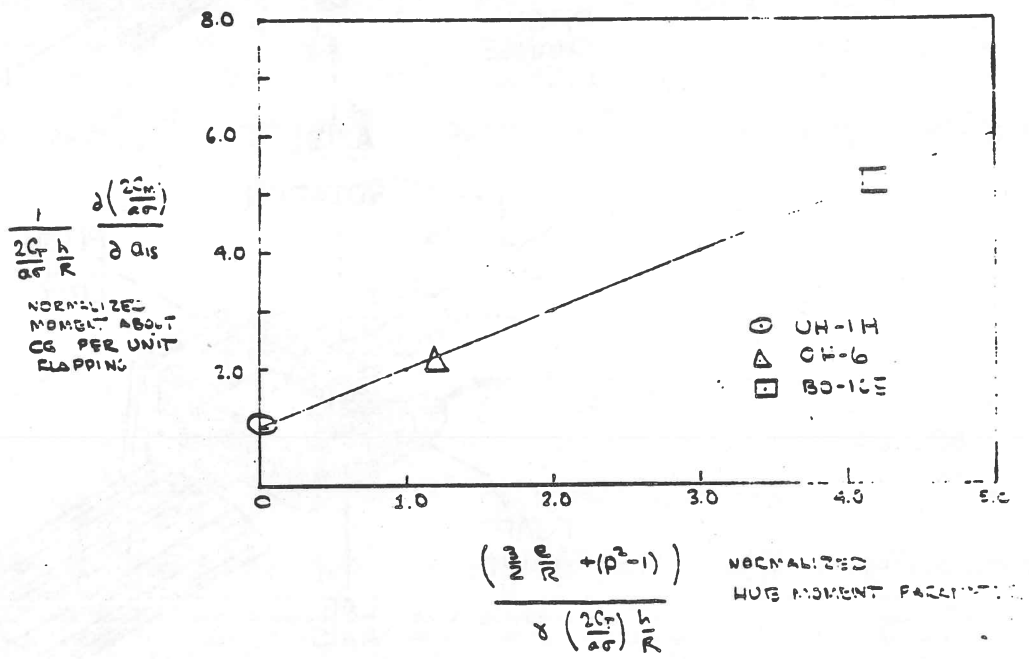

Figure 2. Normalized Moment About Center of Gravity per Unit Flapping Angle.

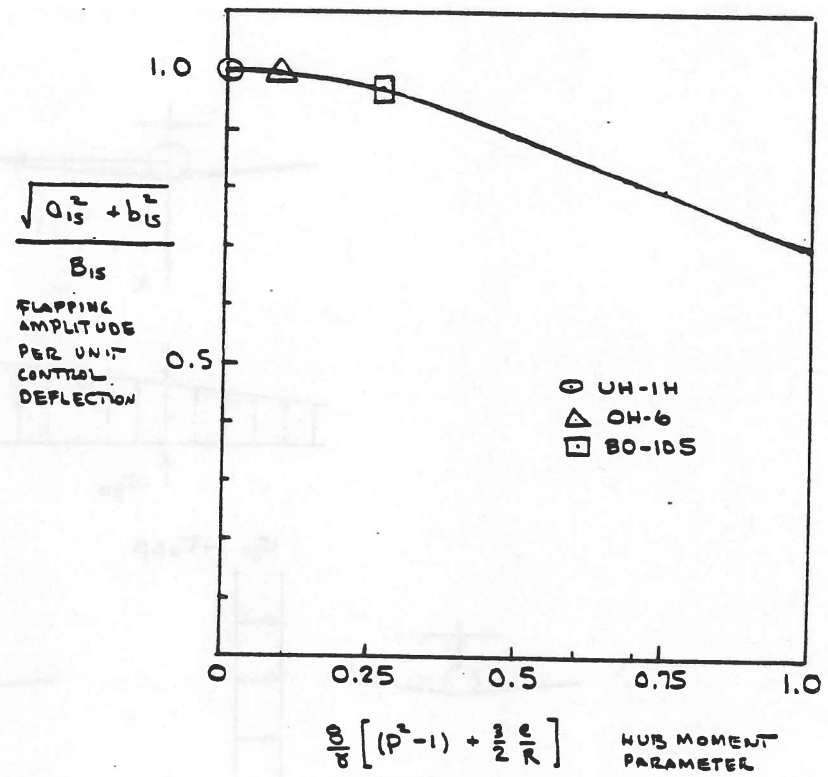

Figure 3. Influence of Hub Moment Parameter on Flapping Amplitude per Unit Control Deflection.

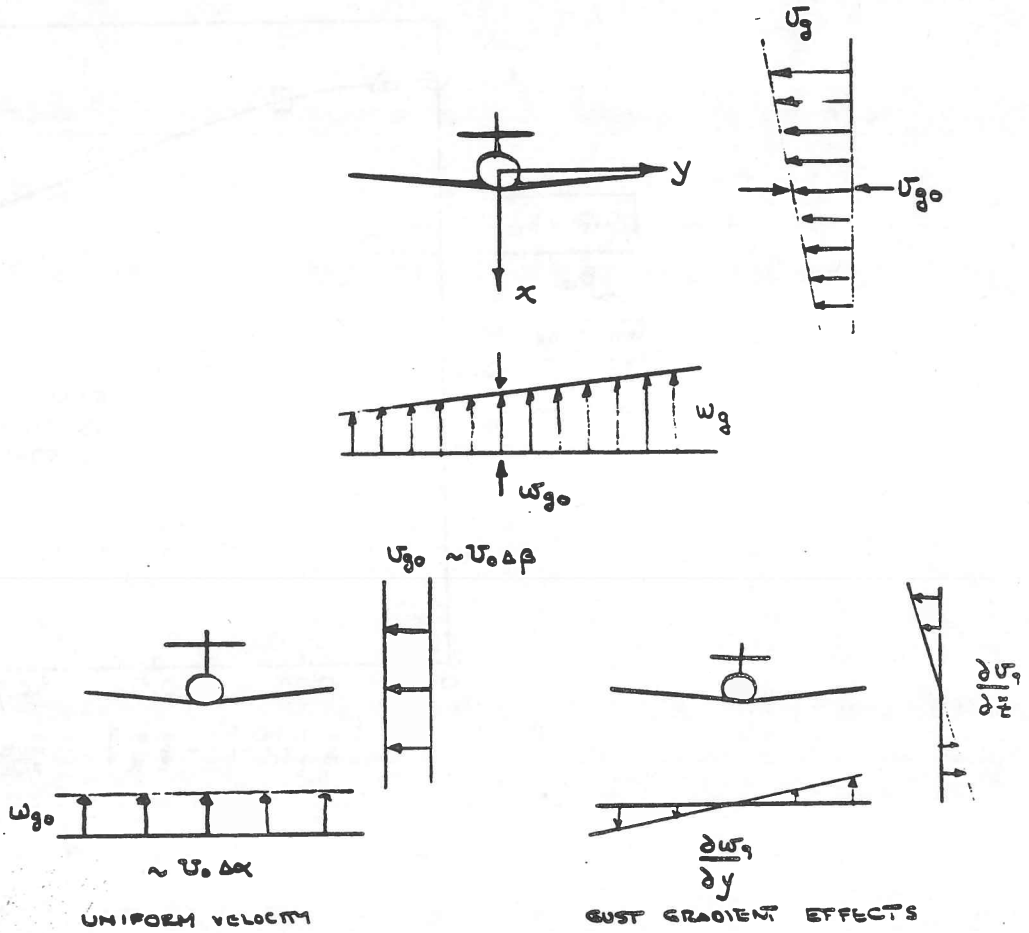

Figure 4. Interpretation of Gust Gradients as Equivalent Motions of Aircraft.

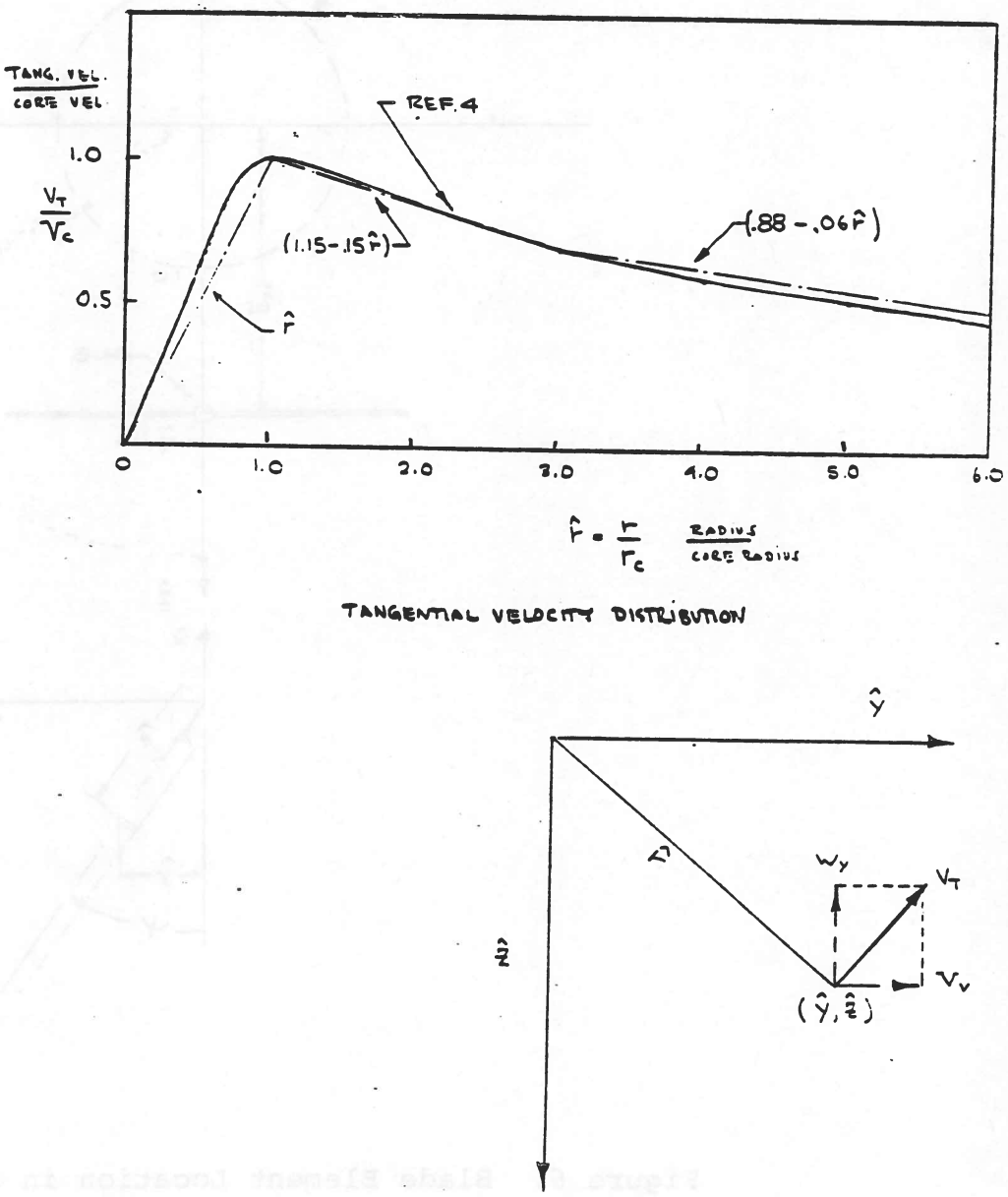

Figure 5. Vortex Flow Field.

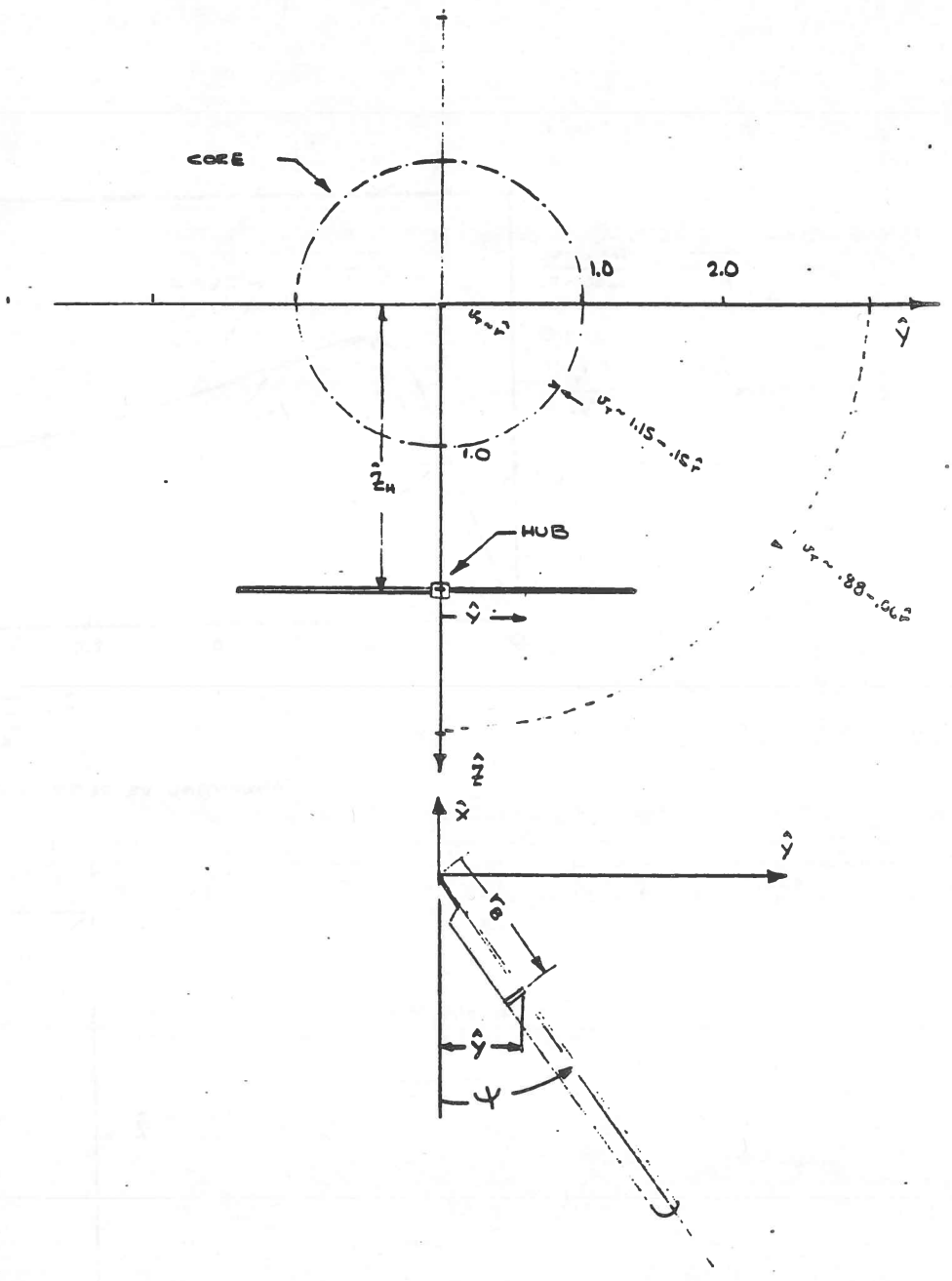

Figure 6. Blade Element Location in Flow Field.

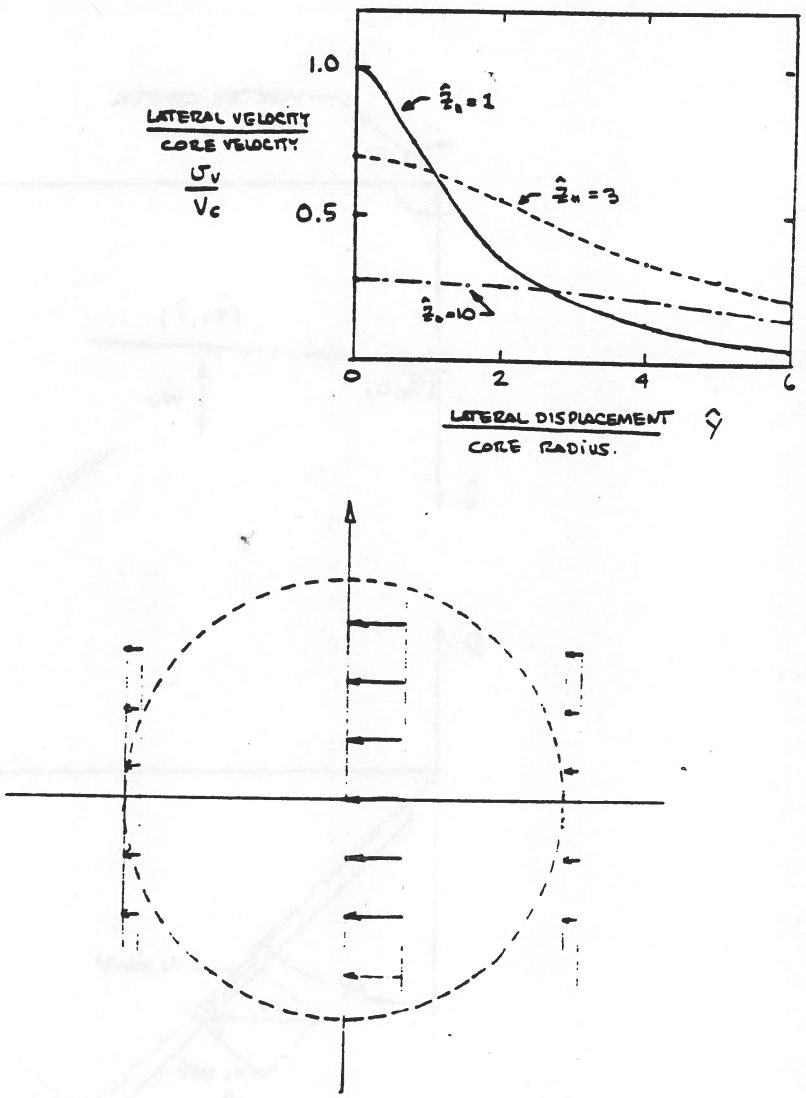

Figure 7. Spanwise Variation in Lateral Velocity Component.

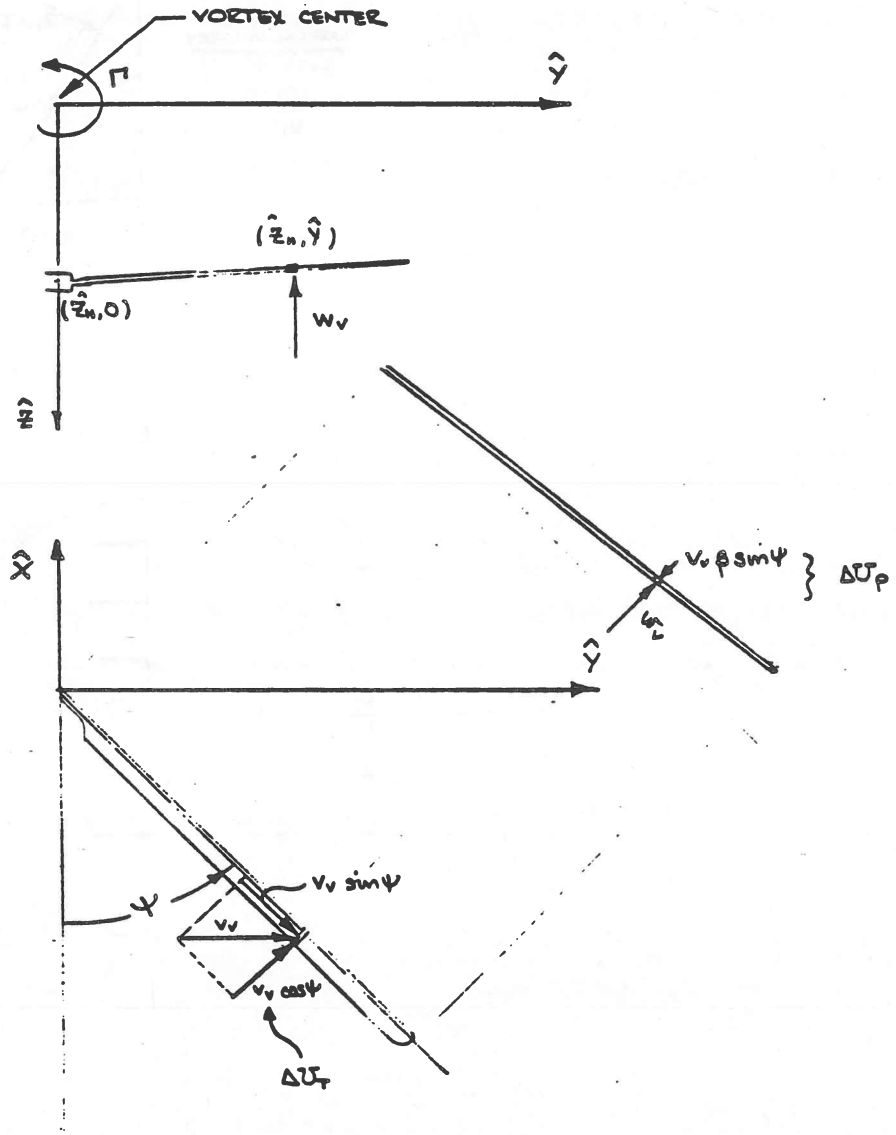

Figure 8. Velocity Components at Blade Element Induced by Vortex Flow Field.

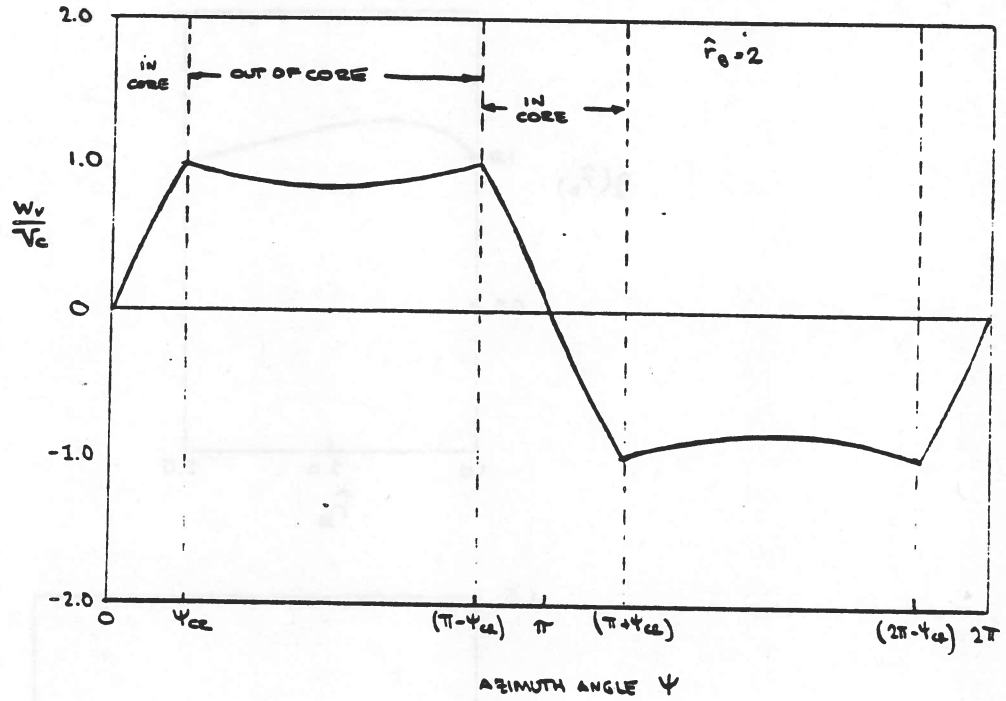

Figure 9. Typical Variation of Vertical Vortex Velocity with Blade Axzimuth Angle at Constant Radial Location on Blade.

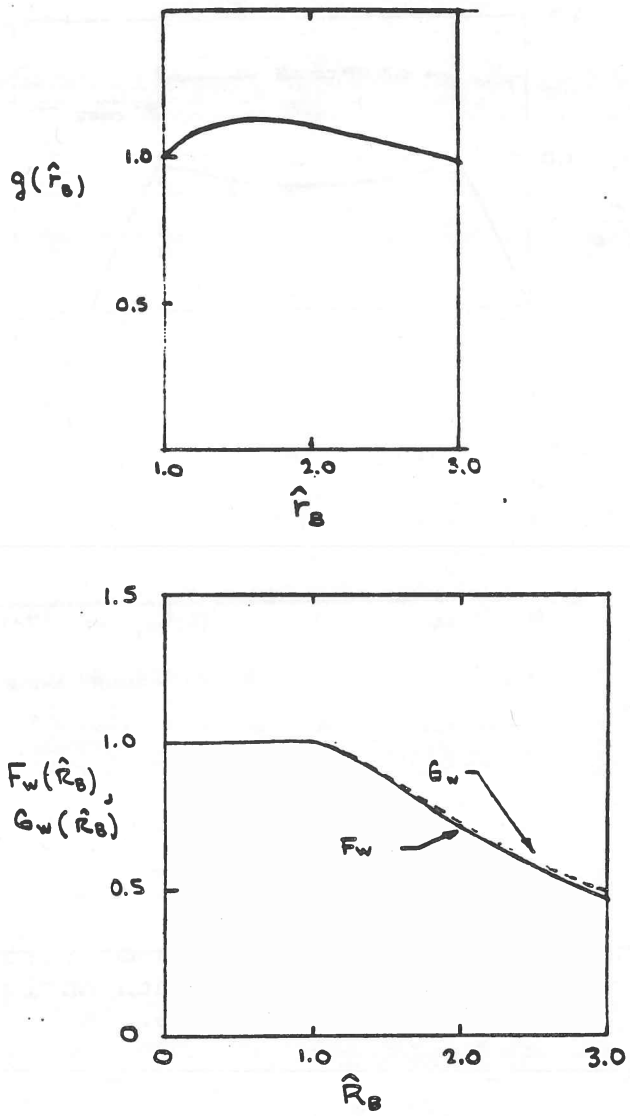

Figure 10. Weighting Factors for Vertical Velocity Input to Rotor Flapping.

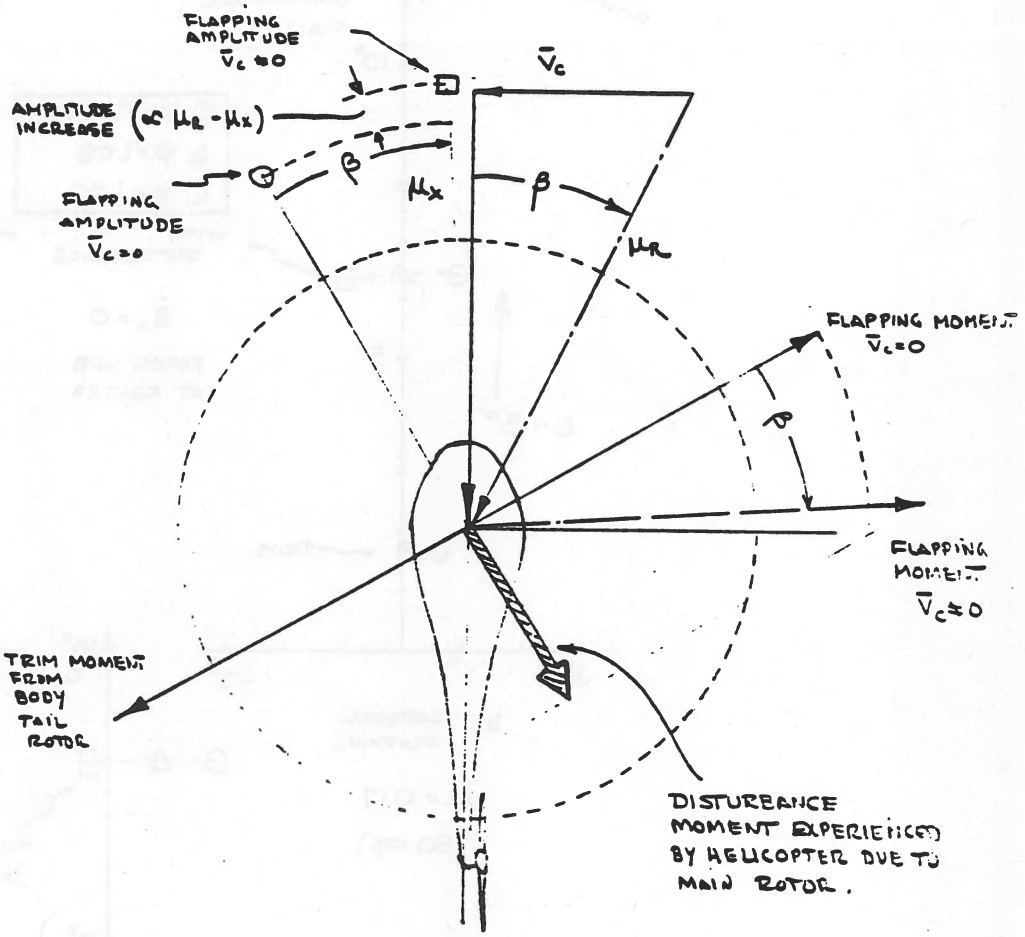

Figure 11. Effect of a Lateral Velocity Disturbance on Rotor Blade Flapping.

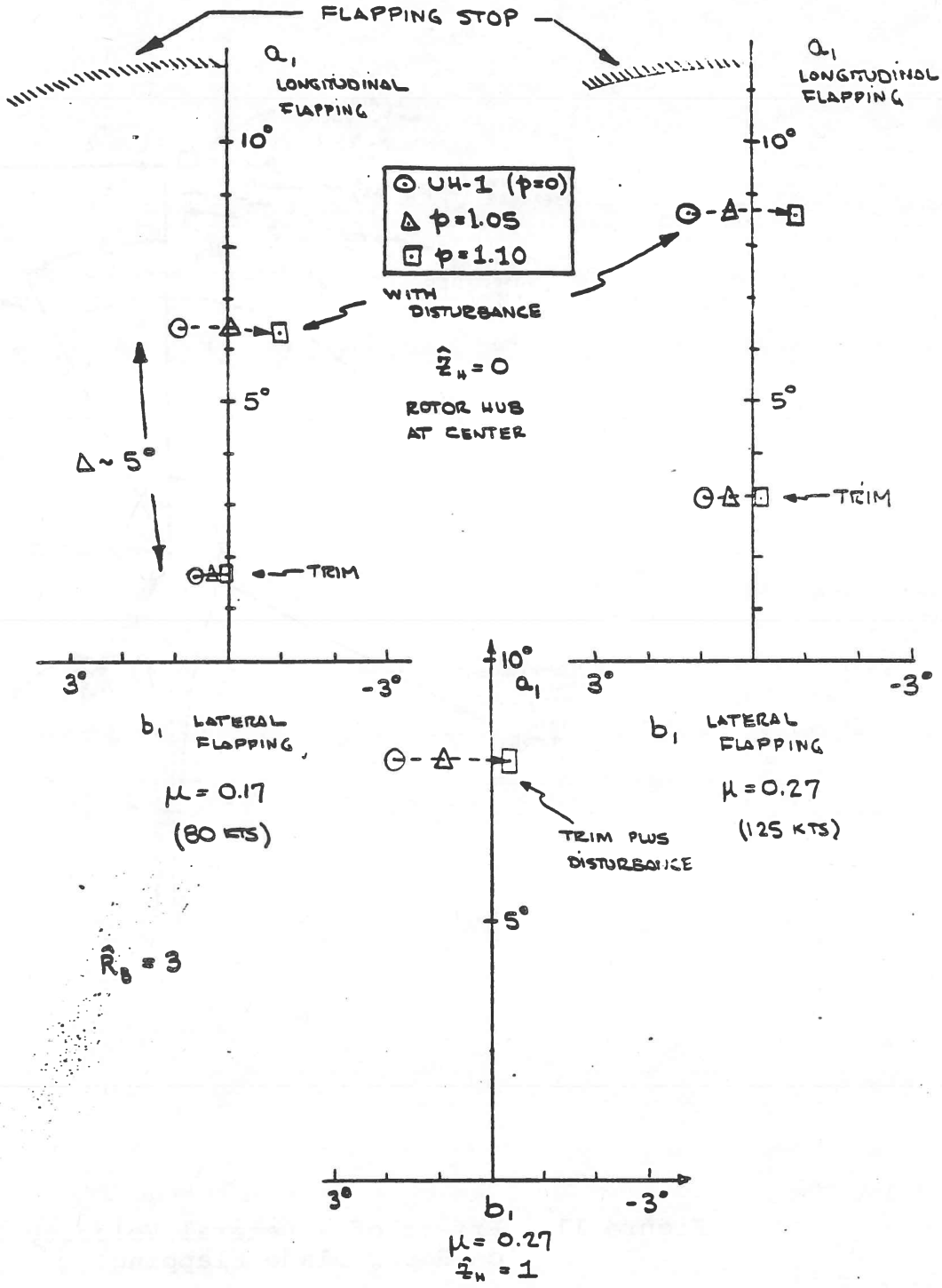

Figure 12. Steady State Flapping Induced by Vortex Flow Field. UH-1H Size Rotor ($\hat{R}_B$ = 3). Flapping Stiffness Varied.

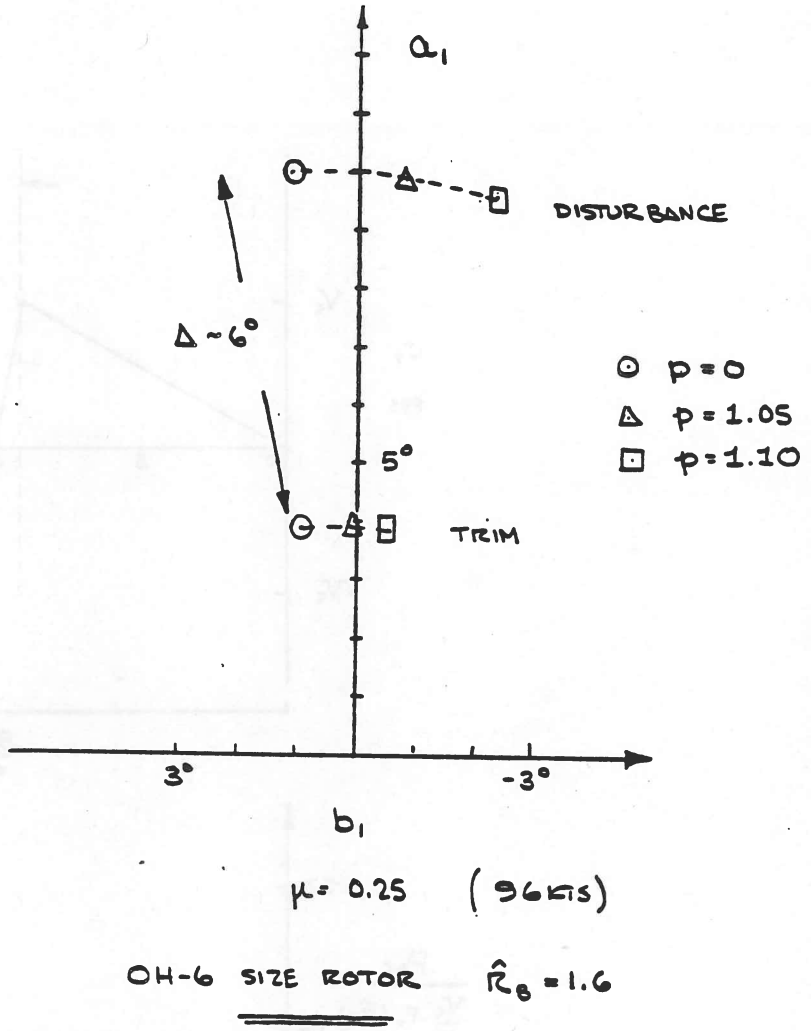

Figure 13. Steady State Flapping Induced by Vortex Flow Field. OH-6 Size Rotor ($\hat{R}_B$ = 1.6). Flapping Stiffness Varied.

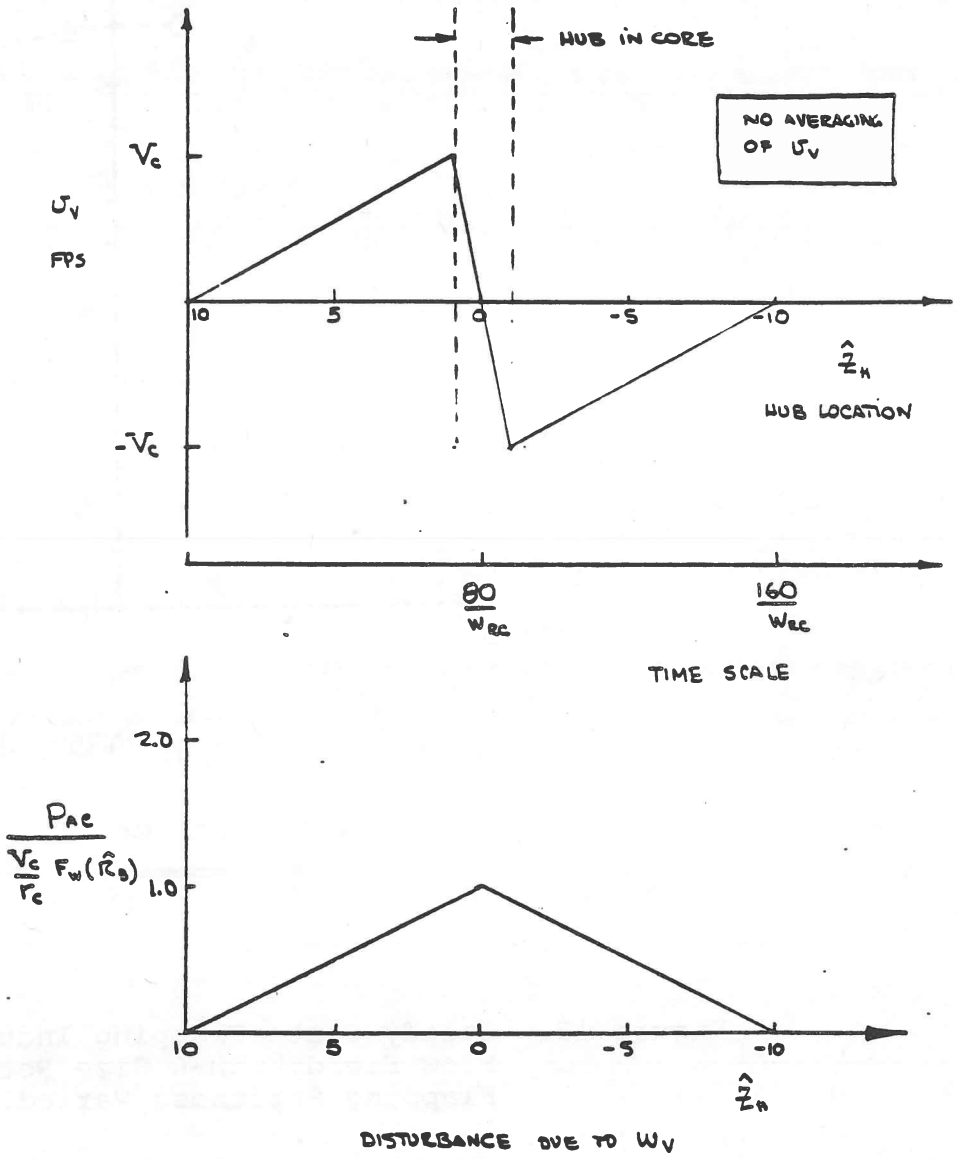

Figure 14. Disturbance Velocities for Dynamic Response Calculations.

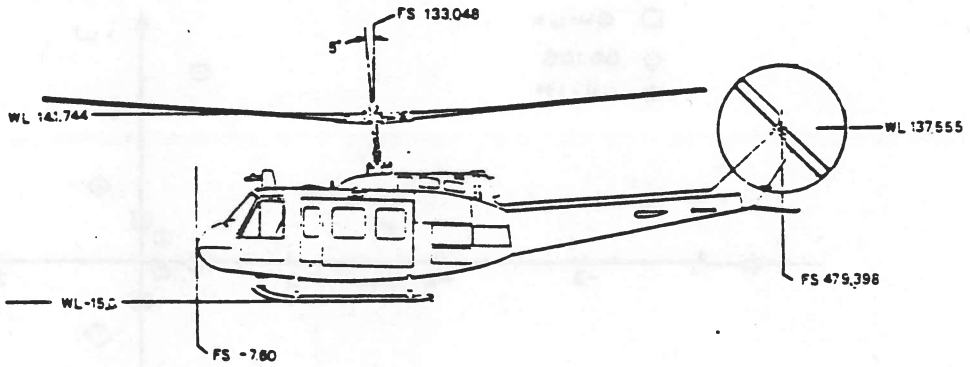

UH-1H

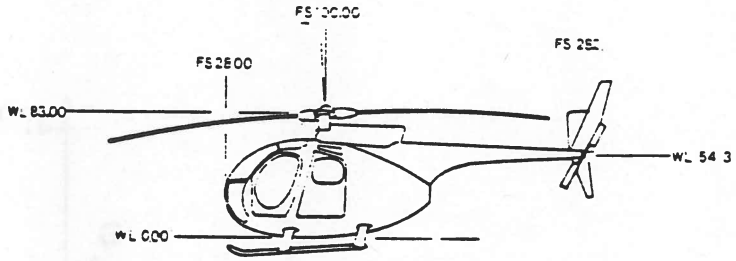

OH-6A

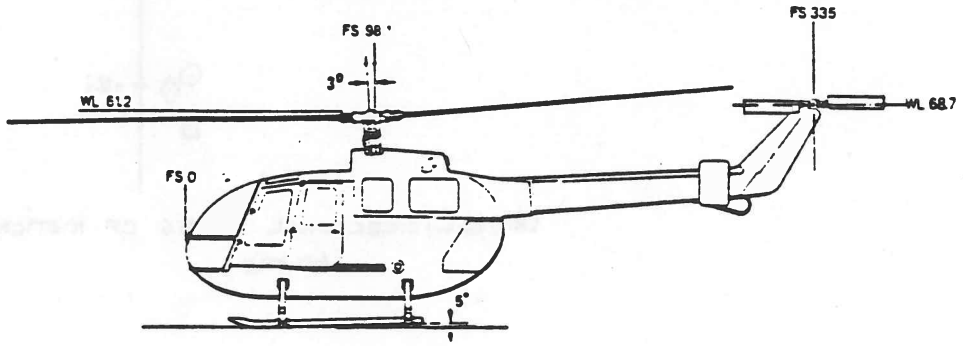

BO-105C

Figure 15. Helicopter Configurations.

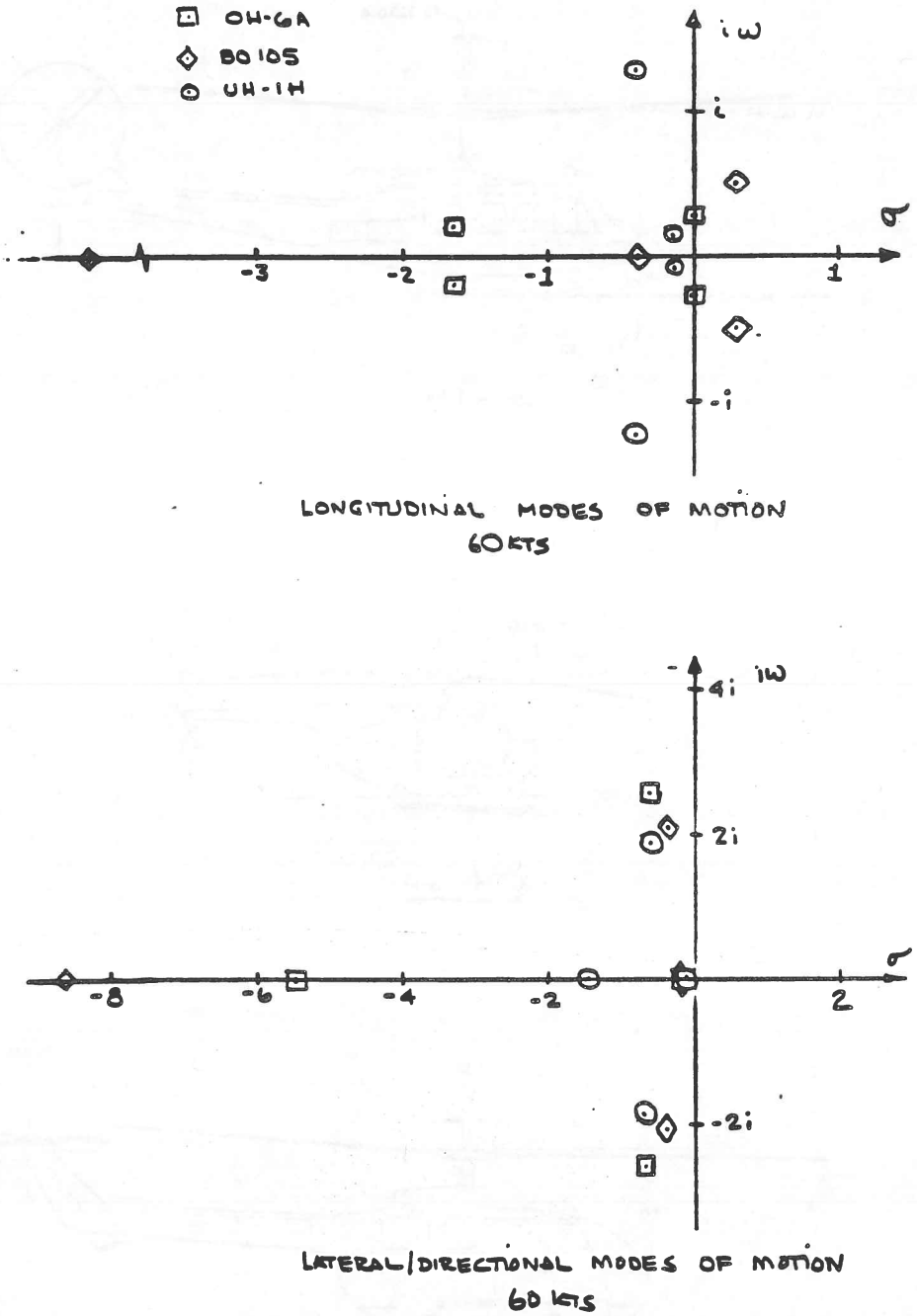

Figure 16. Characteristic Modes of Motion at 60 kts.

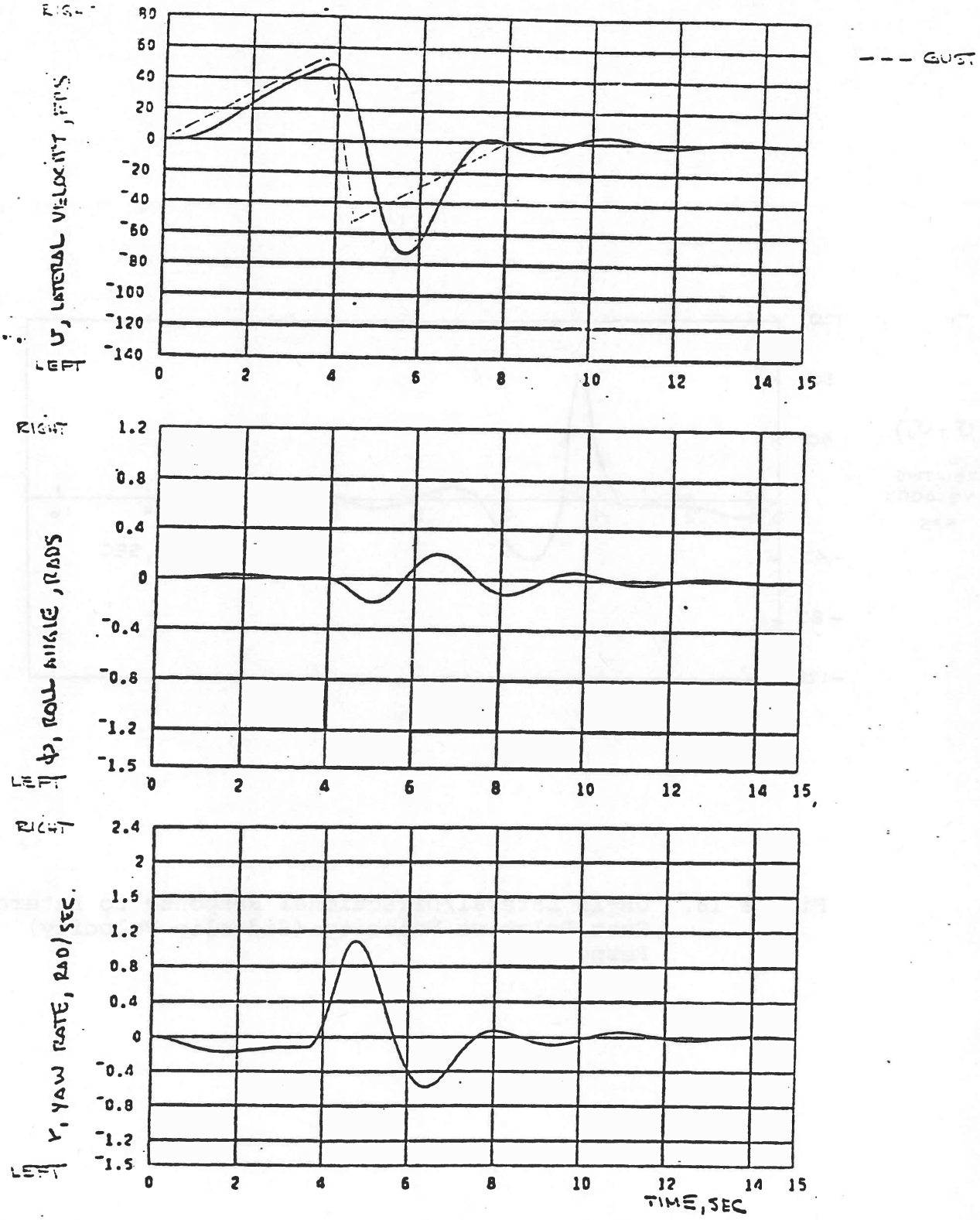

Figure 17. UH-1H Lateral/Directional Response to Lateral Gust. V_o = 60 kts, W_{Rc} = 1200 fpm.

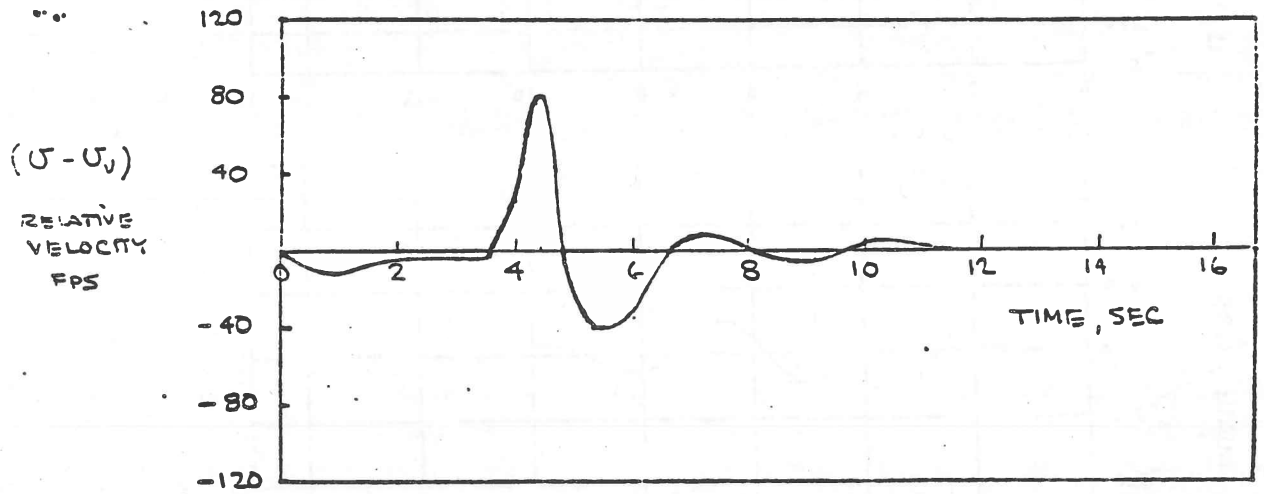

Figure 18. UH-1H Lateral/Directional Response to Lateral Gust Relative Velocity (Sideslip Velocity) Response.

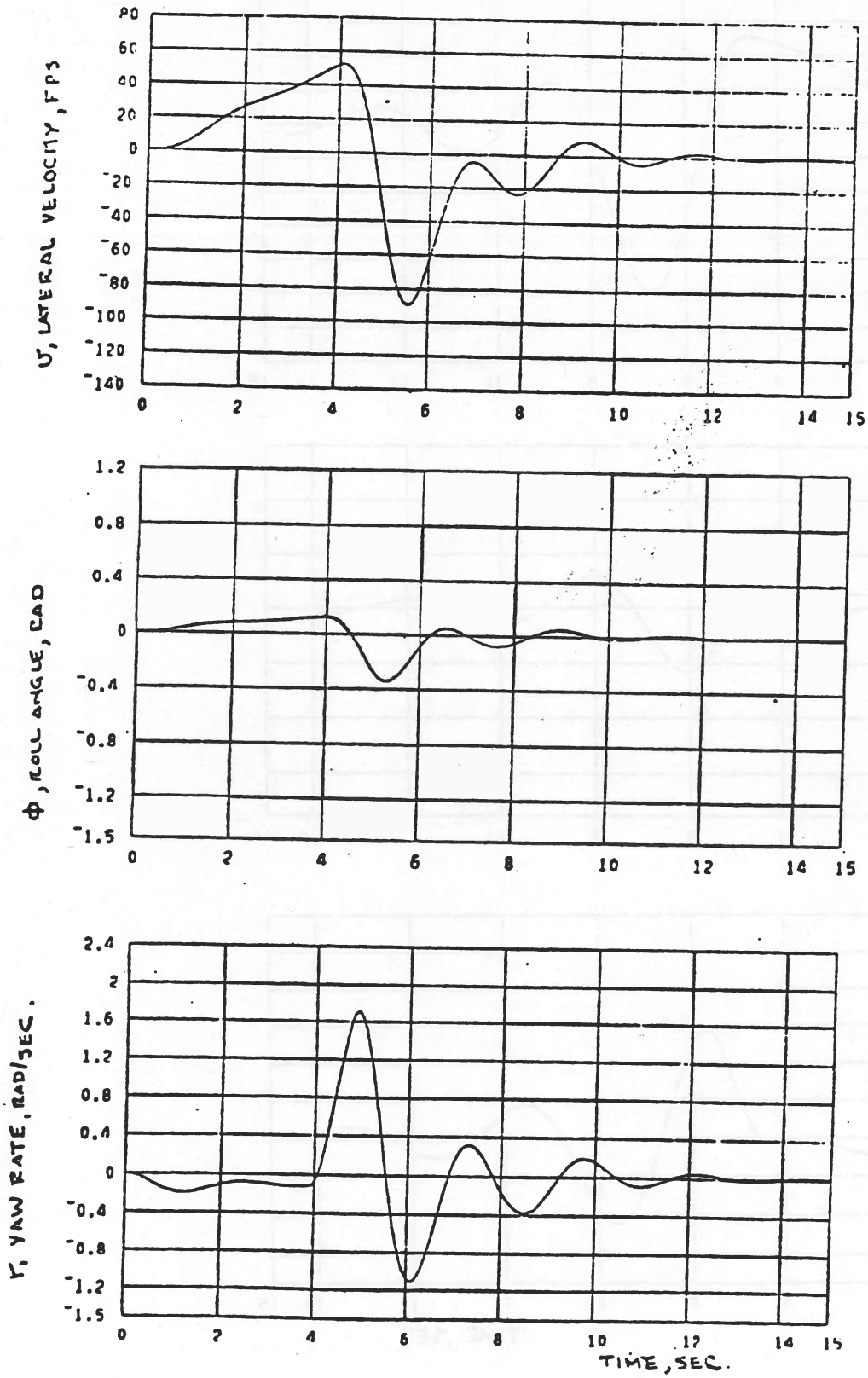

Figure 19. OH-6 Lateral/Directional Response to Lateral Gust. V_o = 60 kts, W_{Rc} = 1116 fpm.

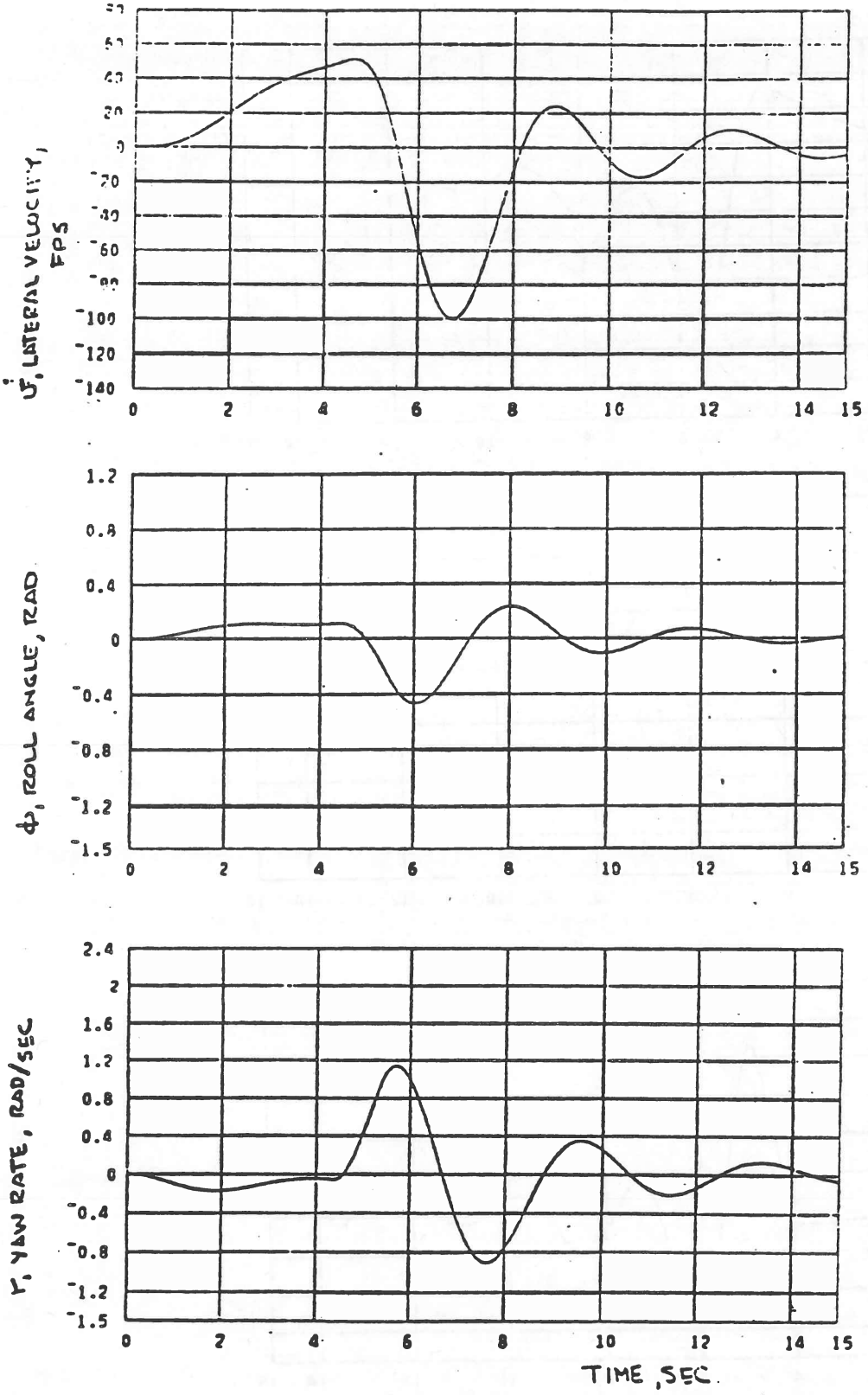

Figure 20. BO-105 Lateral/Directional Response to Lateral Gust. V_o = 60 kts, W_{Rc} = 1000 fpm.

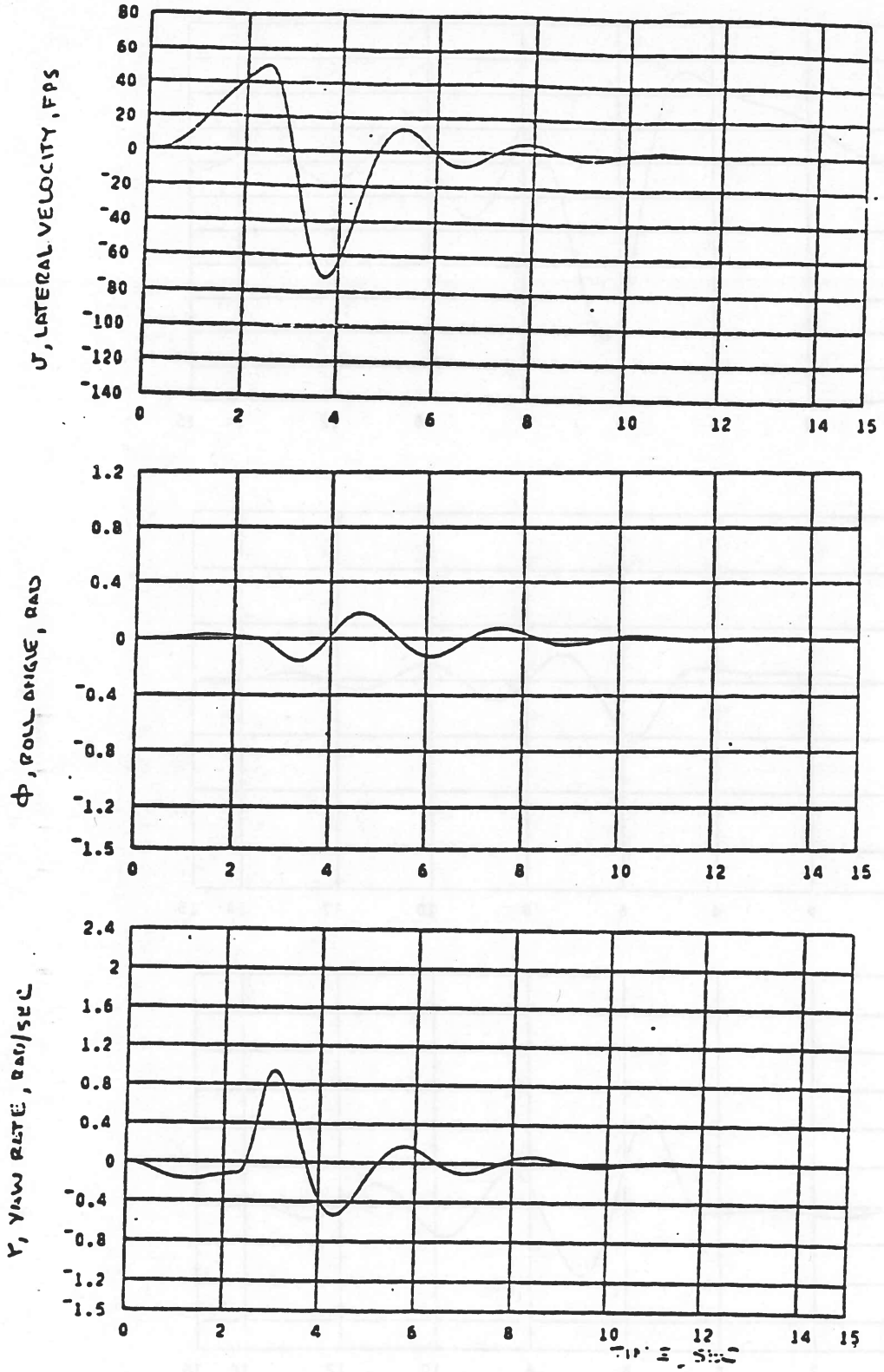

Figure 21. UH-1H Lateral/Directional Response to Lateral Gust. V_o = 100 kts, W_{Rc} = 1900 fpm.

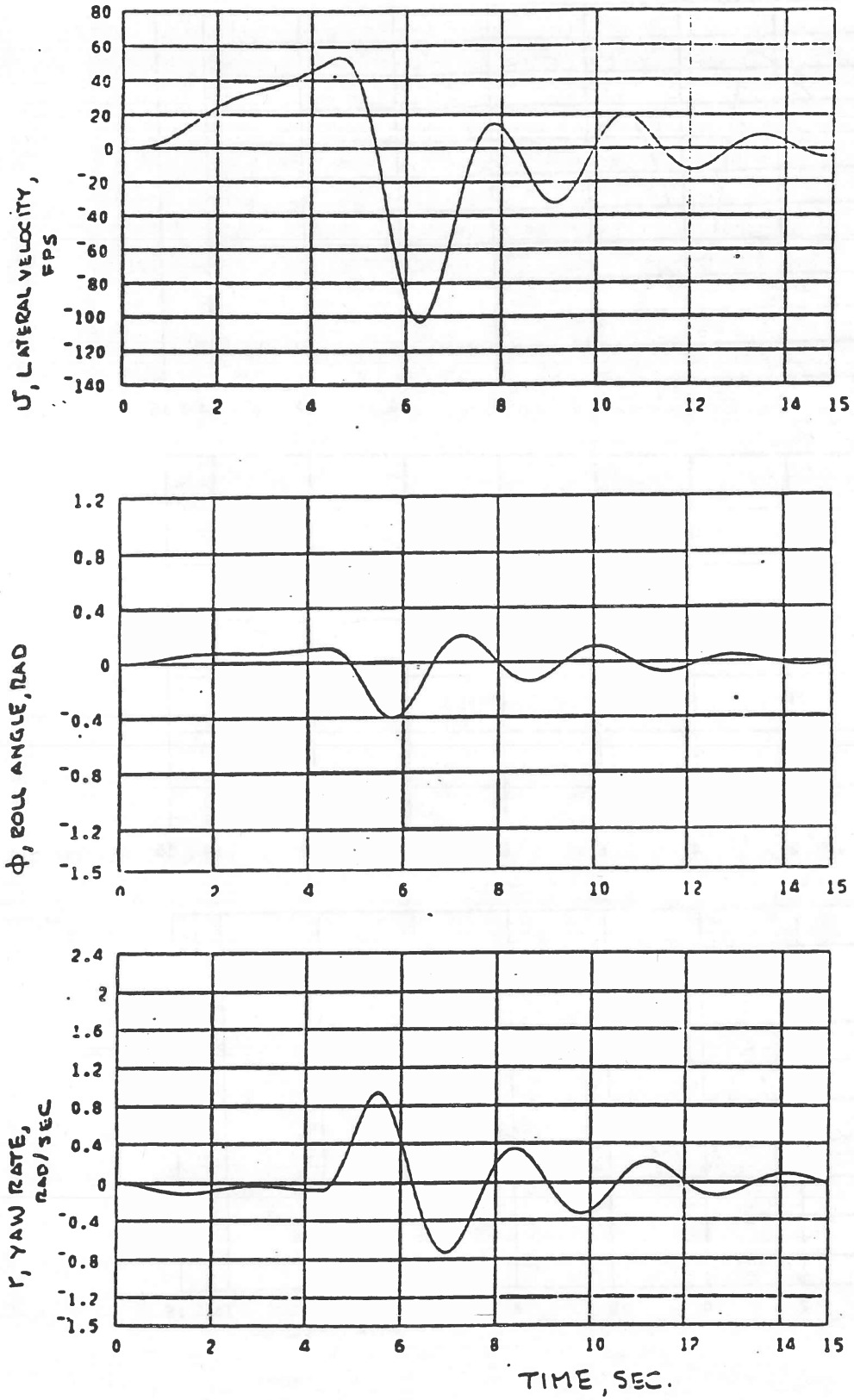

Figure 22. BO-105 Lateral/Directional Response to Lateral Gust. V_o = 100 kts, W_{Rc} = 1000 fpm.

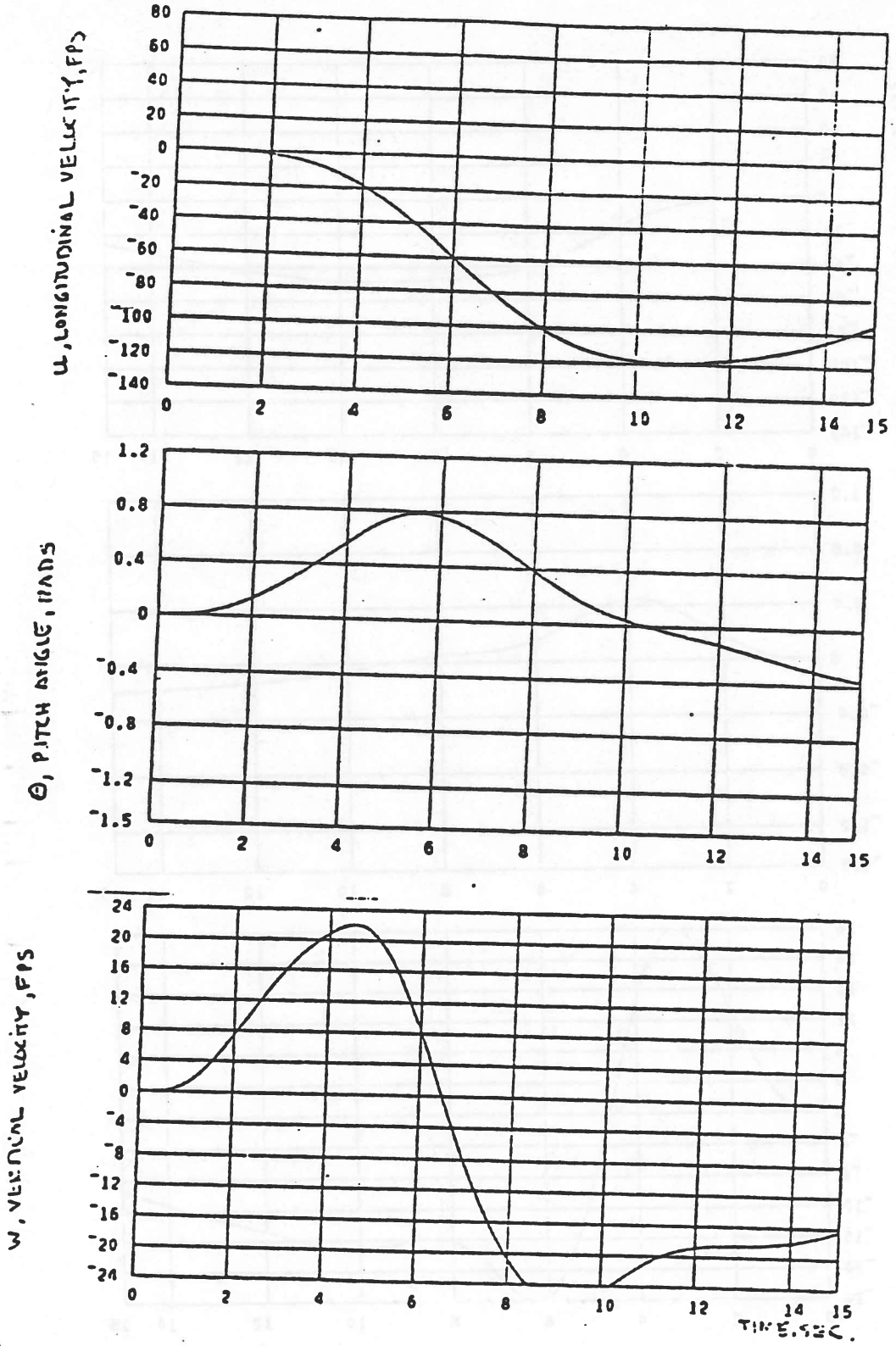

Figure 23. UH-1H Longitudinal Response to Vertical Gust (Aerodynamic Roll). V_o = 60 kts, W_{Rc} = 1200 fpm.

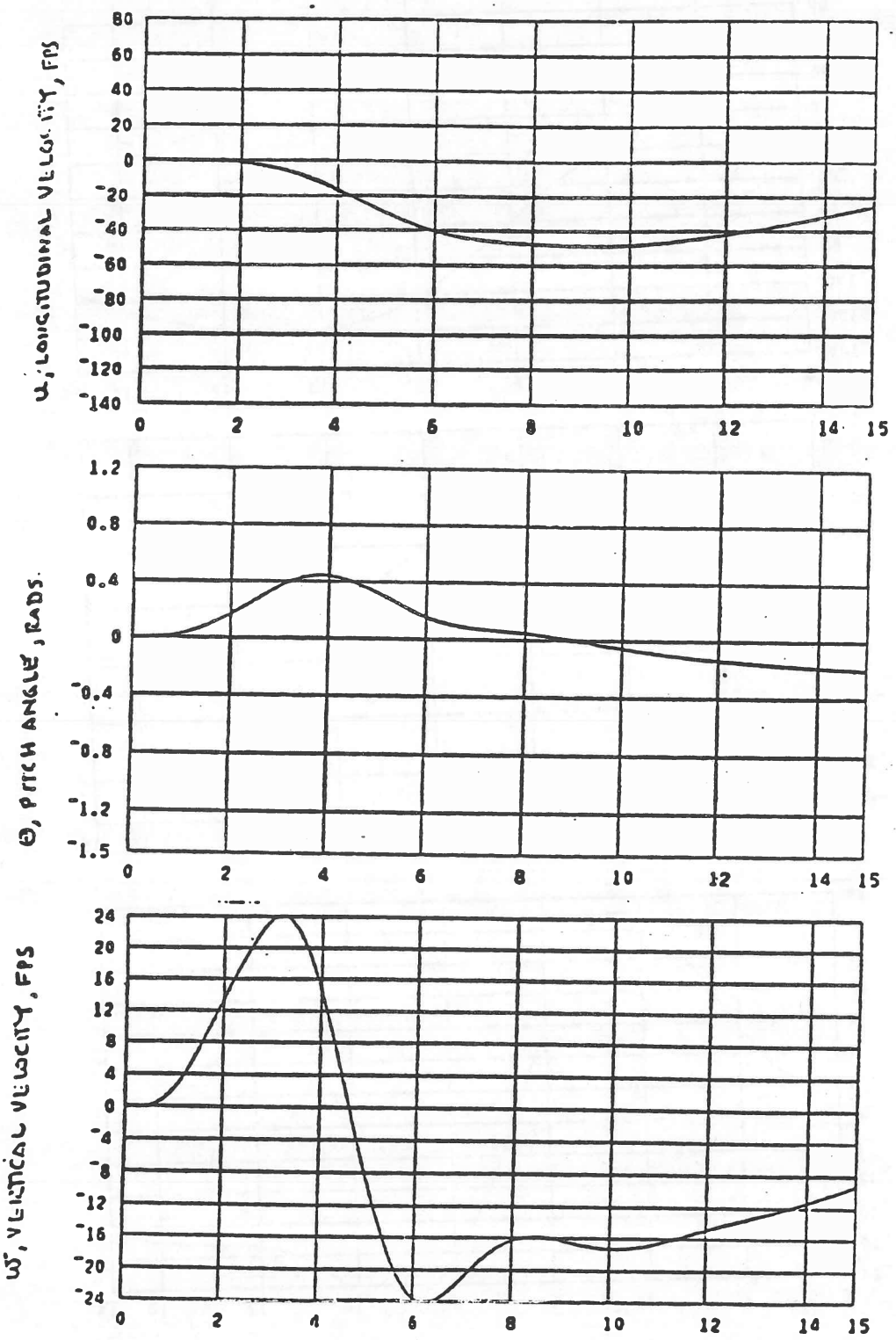

Figure 24. UH-1H Longitudinal Response to Vertical Gust (Aerodynamic Roll). V_o = 100 kts, W_{Rc} = 1900 fpm.

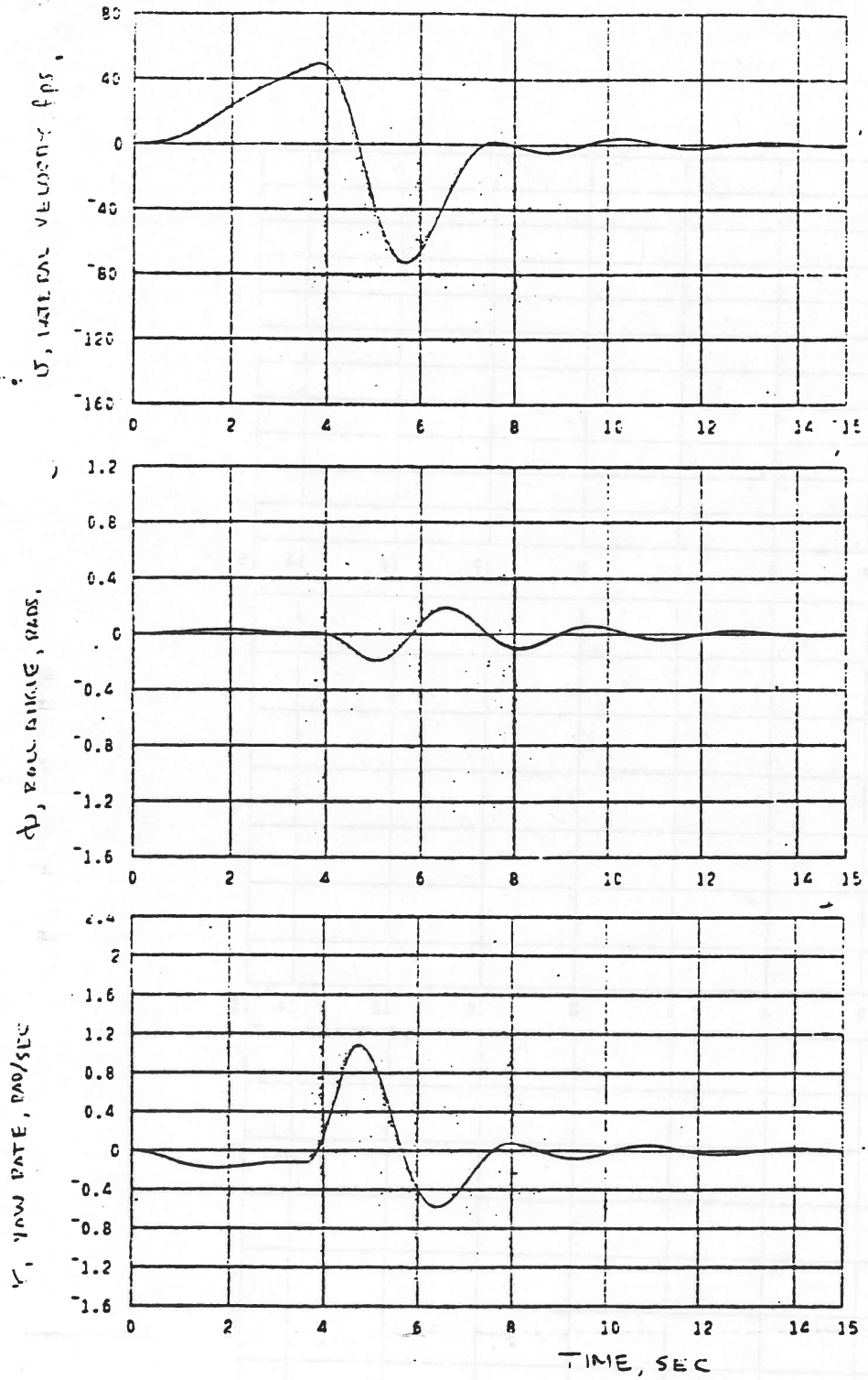

Figure 25. UH-1H Six Degree-of-Freedom Response to Lateral Velocity Component of Vortex Flow Field. V_o = 60 kts, W_{Rc} = 1000 fpm.

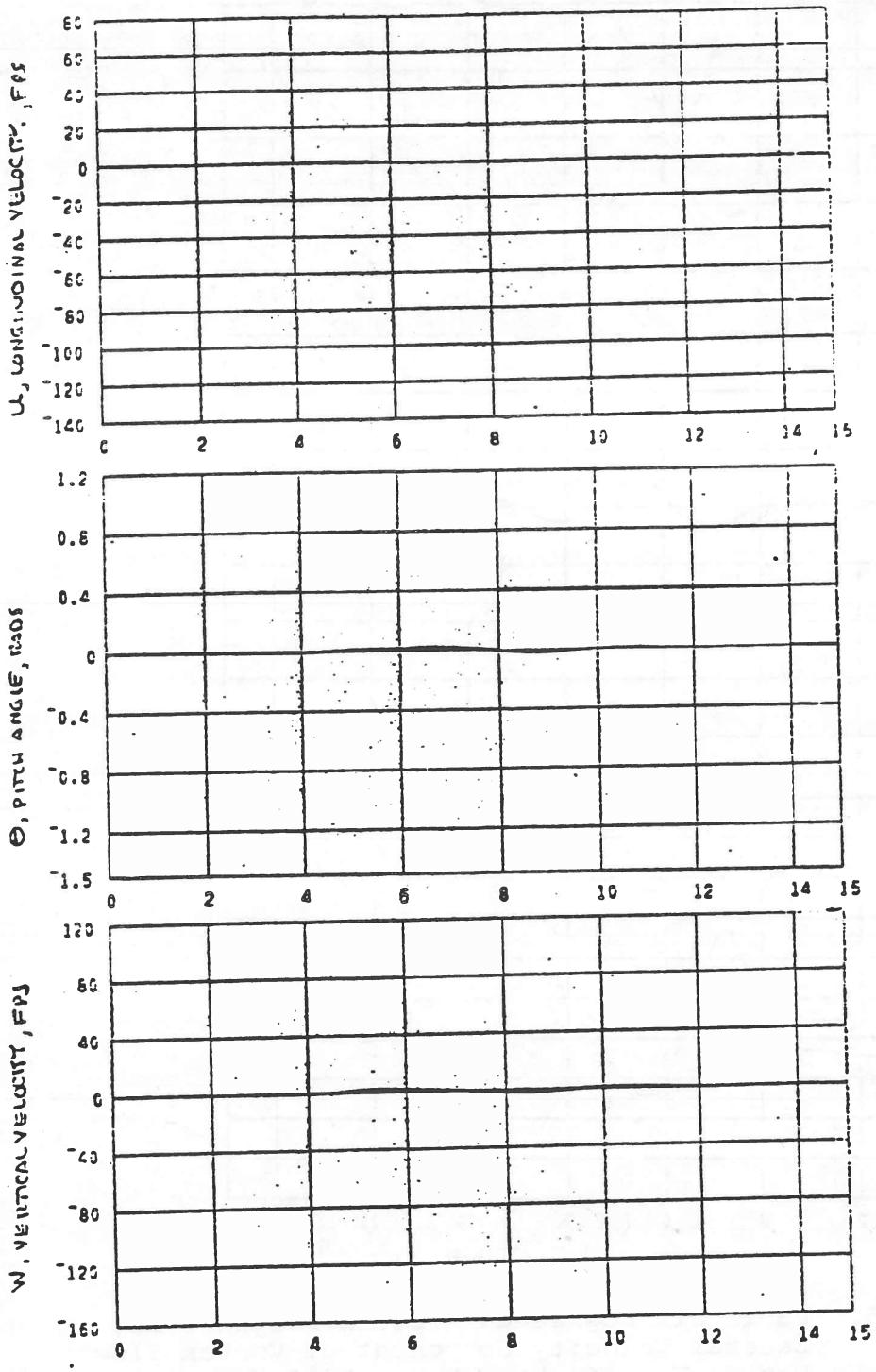

Figure 25. Continued.

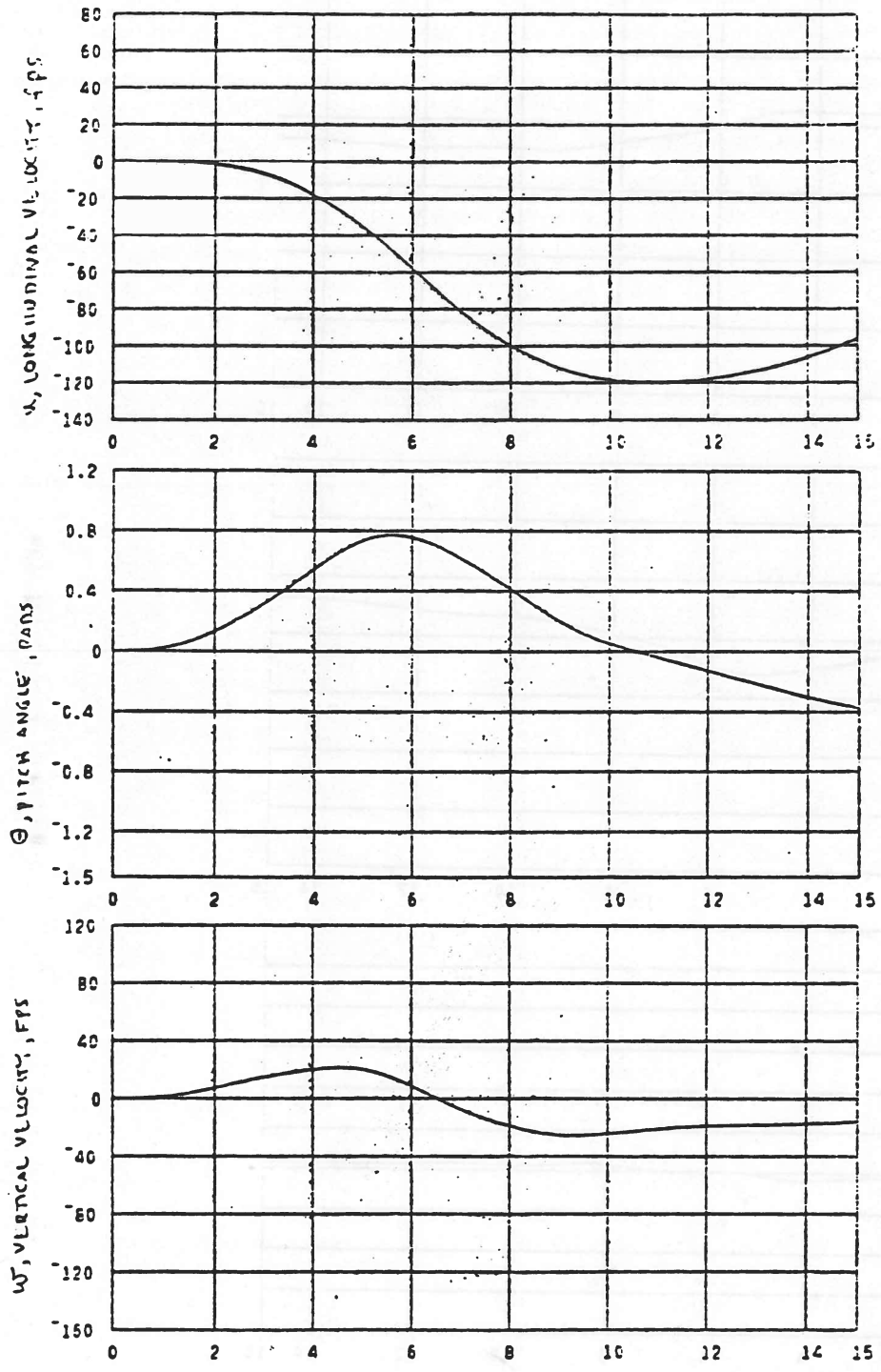

Figure 26. UH-1H Six Degree-of-Freedom Response to Vertical Velocity Component of Vortex Flow Field. V_o = 60 kts, W_{Rc} = 1200 fpm.

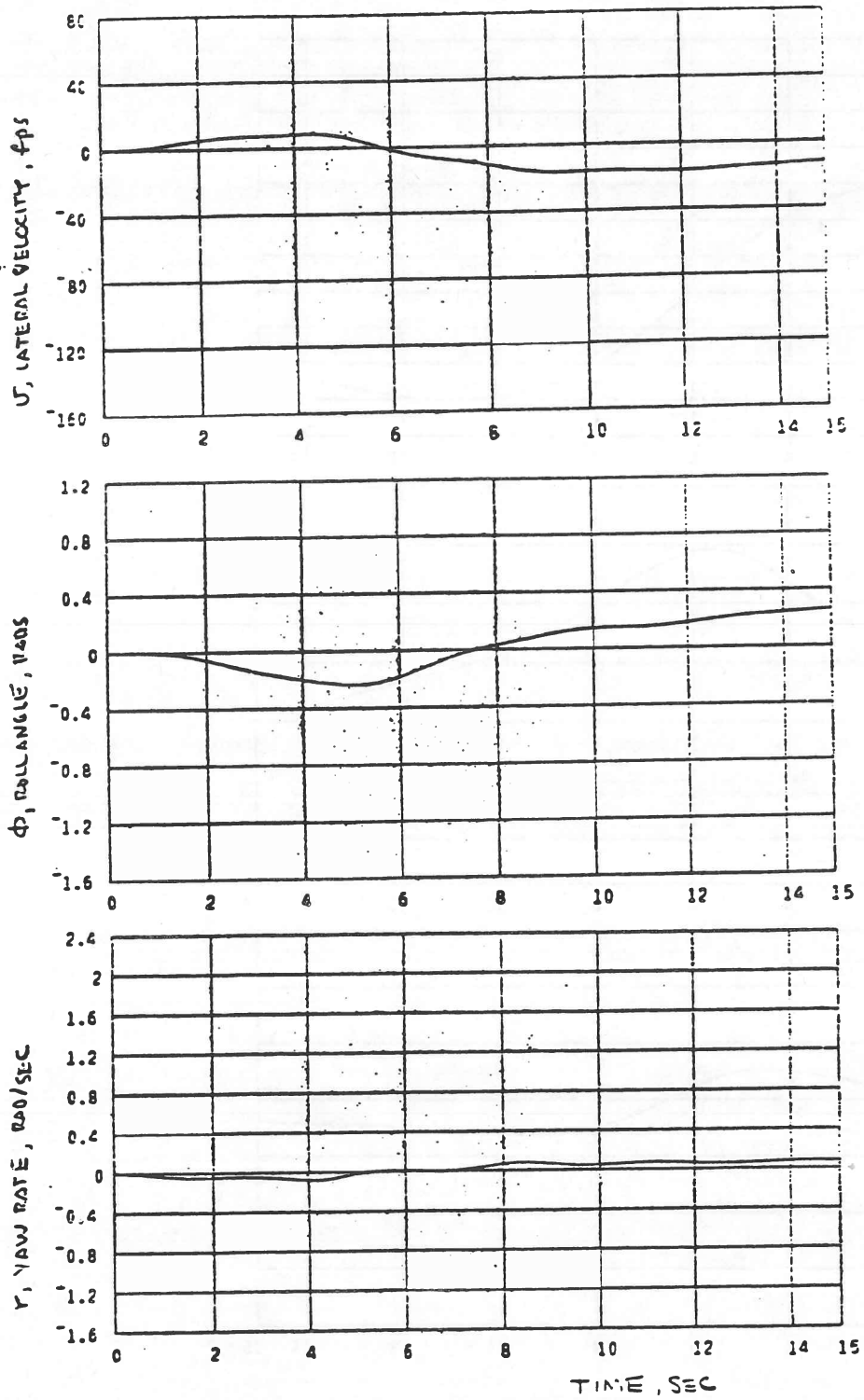

Figure 26. Continued.

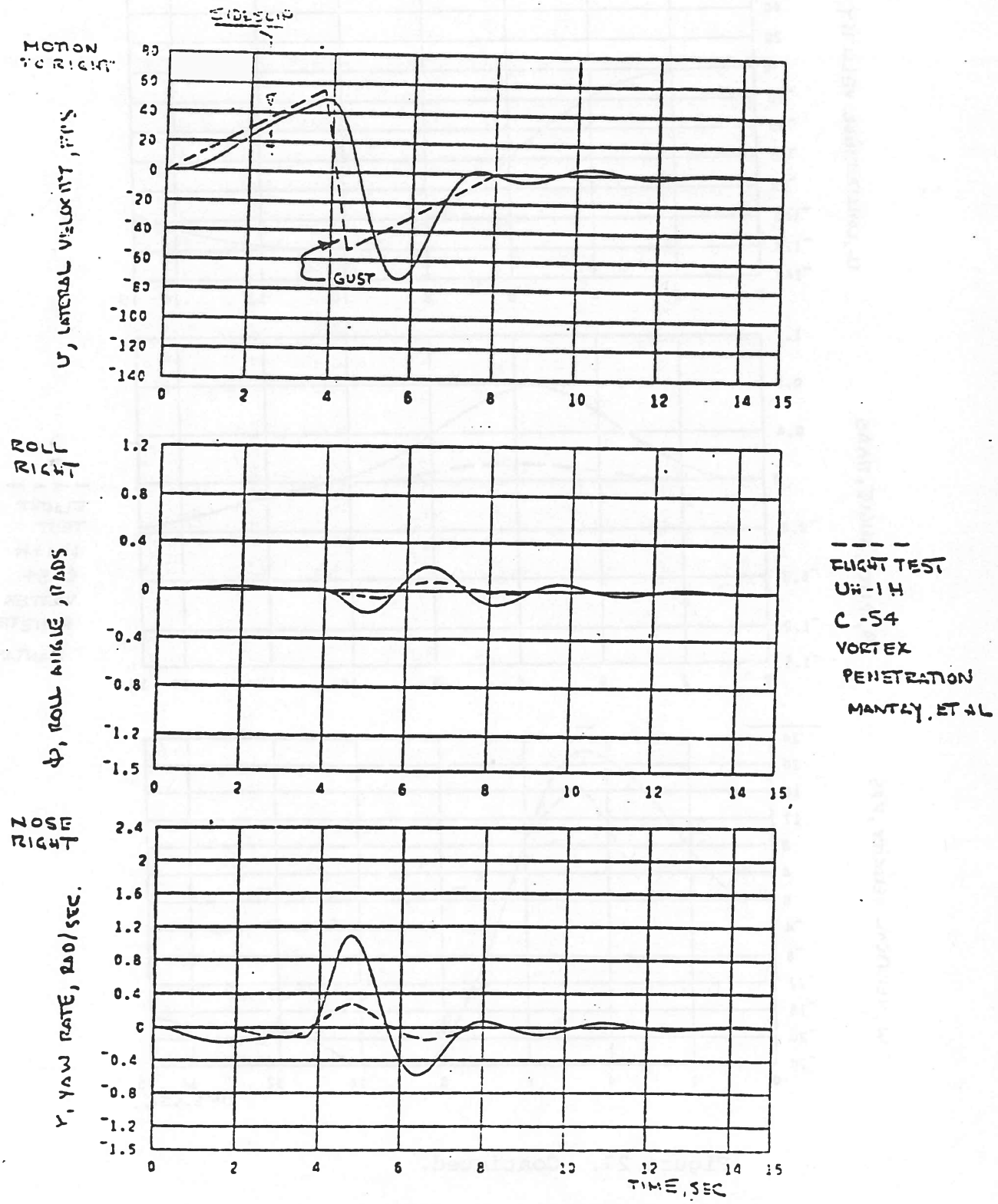

Figure 27. Comparison of Predicted Response to Flight Test, UH-1H. V_o = 60 kts, W_{Rc} = 1200 fpm.

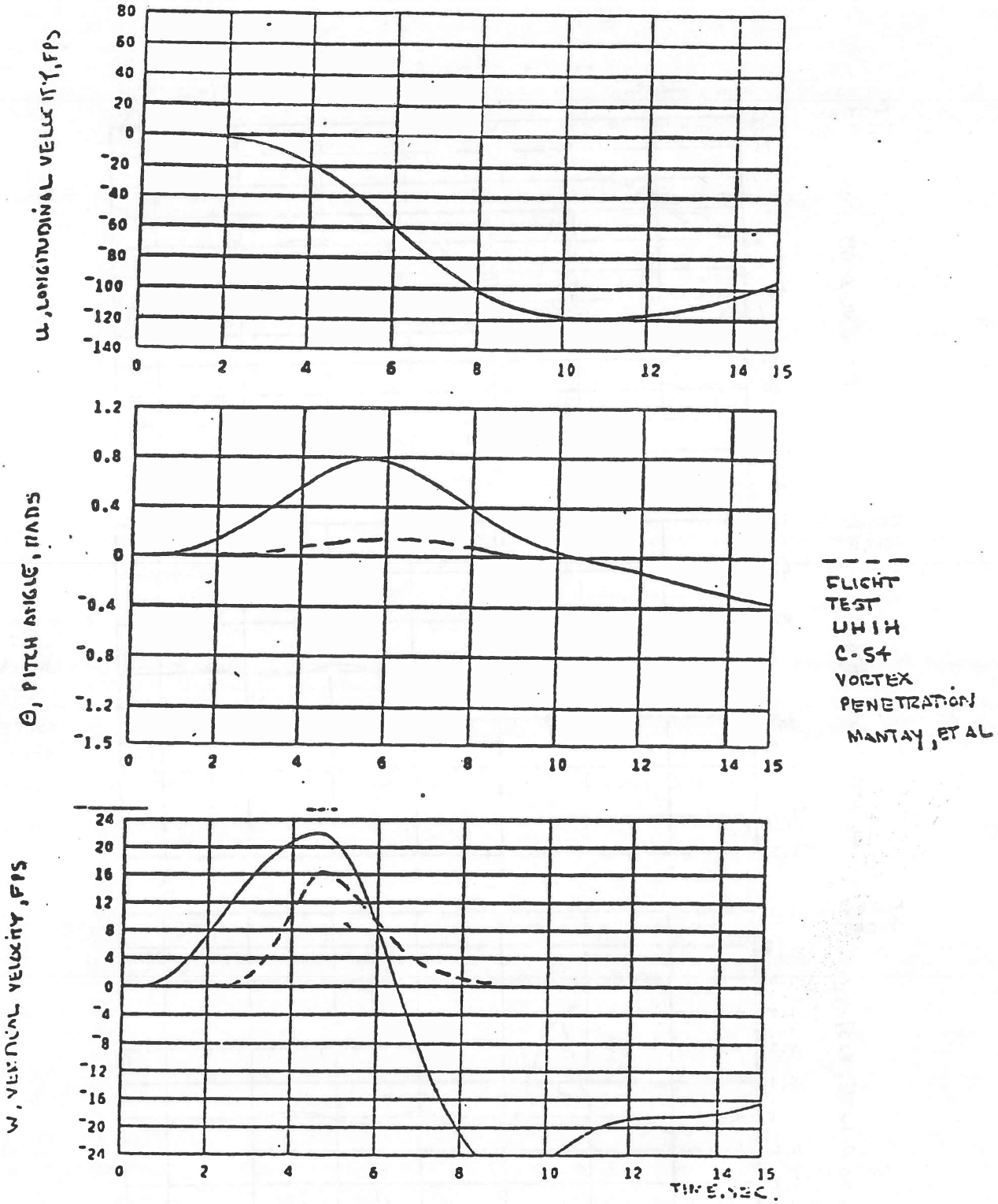

Figure 27. Continued.

APPENDIX

This appendix presents some of the mathematical details associated with the development in the text as well as some notes on the flapping and moment characteristics of helicopter rotors.

Flapping and Moment Characteristics of Helicopter Rotors

In order to provide some understanding of the influence of main rotor type on flapping and moments exerted on a single rotor helicopter, the discussion that follows is a simplified description of rotor blade flapping and moments as influenced by rotor type. It is assumed that a hingeless rotor blade can be represented by a rigid blade with a spring on the flapping hinge. This simple model will demonstrate the essential features of a hingeless rotor. The stiffness of the blade can be represented by the ratio of the rotating hingeless blade natural frequency to rotor RPM denoted by p

$$p = \frac{\omega_{1R}}{\Omega}$$

The frequency ratio can be related to the flapping spring through

$$p^2 = 1 + \frac{K_\beta}{I_B \Omega^2}$$

p is typically about 1.1 for current hingeless rotor helicopters. The moment exerted about the center of gravity of a single rotor helicopter with rotor height h, hinge offset e and spring stiffness K_β can be written as,

$$M \cong \left(Th + \frac{ebM_s\Omega^2}{2} + \frac{b}{2} K_\beta\right) a_{1s}$$

$$L \cong \left(Th + \frac{ebM_s\Omega^2}{2} + \frac{b}{2} K_\beta\right) b_{1s}$$

The first term arises from the tilt of the thrust vector and the second and third terms are hub moments due to hinge offset and hub spring respectively. Only the first term would be present for a centrally-hinged see-saw rotor helicopter. These expressions can be nondimensionalized such that the typical relative sizes of the contributions can be seen.

$$\frac{2C_M}{a\sigma} = \left(\frac{2C_T}{a\sigma}\frac{h}{R} + \frac{3}{2}\frac{e}{R}\frac{1}{\gamma} + \frac{p^2 - 1}{\gamma}\right) a_{1s}$$

Using characteristics typical of modern helicopters

$$\frac{C_T}{\sigma} = 0.08 \quad \frac{e}{R} = .05 \quad a = 5.73$$

$$\gamma = 6 \qquad \frac{h}{R} = 0.3 \quad p = 1.1$$

$$\frac{2C_M}{a\sigma} = (.0084 + .0125 + .035)\, a_{1s}$$

The hub moment due to offset is typically somewhat larger than that due to tilt of the thrust vector and thus a helicopter with hinge offset has about twice the moment about the center of gravity per degree of flapping as a centrally hinged rotor. The hingeless blade produces a hub moment typically about three times that due to thrust tilt and consequently has about four times the moment about the CG per degree of flapping as a see-saw rotor as shown in Figure 2. An equivalent flapping disturbance thus would be expected to produce about twice the moment of that on a see-saw rotor and a hingeless rotor would produce about four times the moment. However as the helicopter moves, flapping induced by body motion would also produce moments in the same ratio so while it is clear that the magnitude of the input due to a gust disturbance is larger for helicopters with offset or hingeless blades it is not obvious whether the motion

will be larger since the angular damping derivatives will be increased as well.

The flapping equations can be expressed as follows (Ref. 7)

$$a_o = \frac{\gamma}{8p^2}\left(\theta_o(1+\mu^2) + \frac{4}{3}\lambda + \frac{2}{3}\mu P_s\right)$$

$$\frac{8}{\gamma}(1-p^2)\,b_{1s} + (1-\frac{\mu^2}{2})a_{1s} = (\frac{8}{3}\,\theta_o + 2\lambda)\,\mu + \frac{P_s}{\Omega} - \frac{16}{\gamma\Omega}\,Q_s - B_{1s}$$

$$-\frac{8}{\gamma}(1-p^2)\,a_{1s} + (1+\frac{\mu^2}{2})\,b_{1s} = \frac{4}{3}\,a_o\mu - \frac{16}{\gamma\Omega}\,P_s - \frac{Q_s}{\Omega} + A_{1s}$$

It may be noted that the presence of the frequency ratio p largely acts to shift the phase of the flapping and due to its typical size p ≅ 1.1 and has little impact on the amplitude of the flapping. That is for $\mu = 0$, for simplicity, the amplitude reduction due to an input, i.e., a term on the right hand side of the equation the flapping amplitude of a hingeless blade is reduced by the factor

$$\frac{1}{\sqrt{1 + (\frac{8}{\gamma}\,(p^2-1))^2}}$$

compared to an articulated blade which can be seen to be small for $p \approx 1.1$. $\gamma \approx 8$. This is illustrated in Figure 3. Thus the amplitude of the flapping of a rotor due to an input or disturbance is to the first order independent of rotor type and then as discussed above, the disturbance moment is largely experienced by a helicopter in proportion to the moment produced per unit flapping angle.

Consider now the effect of shaft rolling velocity on flapping at $\mu = 0$ for simplicity and with p = 1, i.e., the articulated or offset case,

$$a_{1s} = \frac{P_s}{\Omega}$$

$$b_{1s} = -\frac{16}{\gamma\Omega}\,P_s$$

Roll rate of the shaft (P_s) then produces longitudinal as well as a lateral flapping as sketched in Figure A-1. Comparison with the flapping equation for response to a vertical velocity gradient which appears like an effective roll rate shows that the lateral flapping term is absent. This is because the source of the lateral flapping is essentially inertial in nature which can be seen by noting the presence of the Lock number γ in the expression for lateral flapping. Introducing the definition of Lock Number

$$b_{1s} = -\left(\frac{16}{\rho acR^4}\right) I_B \frac{P_s}{\Omega}$$

showing that the lateral flapping is proportional to blade flapping moment of inertia and thus emphasizing its inertial nature. So the effective roll rate due to the vertical velocity gradient of the vortex produces longitudinal flapping in the case of the articulated rotor. For a hingeless rotor some phase shift would be produced and consequently the hingeless rotor would experience a small rolling disturbance in addition to primarily a pitching disturbance from the vertical velocity input.

Mathematical Details

The vertical velocity w_v with the rotor hub located at the vortex center can be expressed as,

$$\bar{w}_v = \bar{V}_c \hat{r}_B \sin\psi \qquad 0 < 4 < \psi_{cR}$$

$$\bar{w}_v = \bar{V}_c \left(1.15 \frac{\sin\psi}{|\sin\psi|} - .15 \hat{r}_B \sin\psi\right) \qquad \psi_{cR} < \psi < \pi - \psi_{cR}$$

$$\bar{w}_v = \bar{V}_c (\hat{r}_B \sin\psi_{cR}) \qquad \pi - \psi_{cR} < \psi < \pi$$

where $\hat{r}_B \sin\psi_{cR} = 1$

and

$$\bar{w}_{vs} = \frac{1}{\pi} \int_0^{2\pi} \bar{w}_v \sin\psi \, d\psi$$

Carrying out the integrals

For $\hat{r}_B < 1$

$$\bar{w}_{vs} = \bar{V}_c \hat{r}_B$$

For $\hat{r}_B < 1$

$$\bar{w}_{vs} = \bar{V}_c \, g(\hat{r}_B)$$

where in the notation of the main body of the report

$$g(\hat{r}_B) = -0.15 \, \hat{r}_B + 1.15 \left(\frac{2}{\pi}\right)\left(\hat{r}_B \sin^{-1} \frac{1}{\hat{r}_B} + \frac{\sqrt{\hat{r}_B^2 - 1}}{\hat{r}_B}\right).$$

Consequently

$$F_w(\hat{R}_B) = \frac{1.15}{\hat{R}_B^4} - .15 + (1.15)\left(\frac{2}{\pi}\right)\left[\sin^{-1} \frac{1}{\hat{R}_B} + \frac{\sqrt{\hat{R}_B^2 - 1}}{\hat{R}_B^4}\right.$$

$$\left. + \frac{5}{3} \frac{(\hat{R}_B^2 - 1)^{3/2}}{\hat{R}_B^3} - \frac{\pi}{2\hat{R}_B^3}\right]$$

and

$$G_w(\hat{R}_B) = \frac{1.15}{\hat{R}_B^3} - .15 + 1.15 \left(\frac{2}{\pi}\right)\left[\sin^{-1} \frac{1}{\hat{R}_B} + \frac{\sqrt{\hat{R}_B^2 - 1}}{2\hat{R}_B^3} + \frac{3}{2} \frac{\sqrt{\hat{R}_B^2 - 1}}{\hat{R}_B^2}\right.$$

$$\left. - \frac{2}{3\hat{R}_B^3} \ln \left|\hat{R}_B + \sqrt{\hat{R}_B^2 - 1}\right| - \frac{\pi}{2\hat{R}_B^3}\right]$$

Numerical values of these terms are given in Figure 12. The integrals appearing in the determination of the lateral velocity terms can be evaluated as follows:

a.) F_{2c}

$$F_{2c} = \frac{1}{\pi} \int_o^{2\pi} \frac{\cos^2\psi \, d\psi}{\sqrt{\hat{z}_H^2 + \hat{r}_B^2 \sin^2\psi}}$$

let,

$$k^2 = \frac{\hat{r}_B^2}{\hat{z}_H^2 + \hat{r}_B^2}$$

and

$$\cos\psi = x$$

$$\sin\psi = \sqrt{1 - x^2} \quad \text{(1st quadrant only)}$$

Therefore,

$$F_{2c} = -\frac{4}{\pi} \frac{1}{\hat{z}_H^2 + \hat{r}_B^2} \int_1^o \frac{x^2 dx}{\sqrt{1 - x^2}\sqrt{1 - k^2x^2}}$$

The integral can be expressed in terms of complete elliptic integrals of the first and second kind $F(\pi/2,k)$, $E(\pi/2,k)$ as

$$F_{2c} = -\frac{4}{\pi} \frac{1}{\hat{z}_H^2 + \hat{r}_B^2} \left(\frac{1}{k^2}\right) \left(F\left(\frac{\pi}{2},k\right) - E\left(\frac{\pi}{2},k\right)\right)$$

Similarly

$$F_{2s} = F_{2c} - \frac{4}{\pi} \frac{1}{\sqrt{\hat{z}_H^2 + \hat{r}_B^2}} F\left(\frac{\pi}{2},k\right)$$

$$F_{2c2s} = F_{2c} - F_{2s}$$

$$F_{4c} = \frac{8}{3\pi} \frac{1}{\hat{r}_B k^3} \left[\left(1 + \frac{k^2}{2}\right) F\left(\frac{\pi}{2},k\right) - (1 + k^2) E\left(\frac{\pi}{2},k\right)\right]$$

$$F_{4s} = F_{2s} - F_{2c2s}$$

The limiting values of these integrals as $\hat{r} \to 0$, $\hat{z}_H = 1$ are the k^*. These integrals are plotted in Figure A-2. It can be seen from the graphs that it is quite reasonable to approximate these functions as linearly dependent upon $\hat{r}_B$ in order to determine integrals of these functions.

For $\hat{z}_H = 1$, let

$$F_{NcMs} = k^*_{NcMs} - \alpha_{NcMs} \hat{r}_B$$

where α is obtained from the graphs.

Then

$$AF_{NcMs} + k^*_{NcMs} B$$

$$= (A + B)\, k^*_{NcMs} - \alpha_{NcMs} A \hat{r}_B$$

and so

$$I^b_{NcMs} = (A + B)\, k^*_{NcMs} - \frac{b}{(b + 1)} \alpha_{NcMs} \hat{AR}_B$$

The values of α_{NcMs} approximated from Figures A-2 are:

$$\alpha_{2c} = .11 \qquad \alpha_{4c} = .069 \qquad \alpha_{2c2s} = 0.4$$

$$\alpha_{2s} = .207 \qquad \alpha_{4s} = .377$$

It may be noted that the first term in each of the integrals represents the effect of a uniform lateral velocity and the second term is the averaging effect due to the distribution of v_v across the rotor. For vertical velocity terms the first term is the effect of a linear distribution of w_v across the rotor and the second term is due to the departure from the linear distribution.

Two other integrals are required,

$$\frac{1}{\pi} \int_0^{2\pi} \frac{\cos^2\psi \, d\psi}{\hat{z}_H^2 + \hat{r}_B^2 \sin^2\psi} \quad \text{and} \quad \frac{1}{\pi} \int_0^{2\pi} \frac{\sin^2\psi \cos^2\psi \, d\psi}{\hat{z}_H^2 + \hat{r}_B^2 \sin^2\psi}$$

From Dwight (858.553),

$$\frac{1}{\pi}\frac{1}{\hat{z}_H^2}\int_o^{2\pi}\frac{\cos^2\psi\, d\psi}{1+\epsilon^2\sin^2\psi} = \frac{2}{\hat{z}_H^2+\sqrt{\hat{z}_H^4+\hat{z}_H^2\hat{r}_B^2}}$$

$$\epsilon = \frac{\hat{r}_B}{\hat{z}_H}$$

$$\frac{1}{\pi}\frac{1}{\hat{z}_H^2}\int_o^{2\pi}\frac{\sin^2\psi\cos^2\psi\, d\psi}{1+\epsilon^2\sin^2\psi} = \frac{1}{2\hat{z}_H+\hat{r}_B^2+2\sqrt{\hat{z}_H^2+\hat{z}_H^2\hat{r}_B^2}}$$

For $\hat{z}_H^2 = 1$

$$I_{2c}^{*2} = \frac{4A}{\hat{R}_B^2}\left[\sqrt{1+\hat{R}_B^2}-1-\ln\frac{\left(\sqrt{1+\hat{R}_B^2}+1\right)}{2}\right]+B$$

$$I_{2c2s}^{*2} = \frac{2A}{\hat{R}_B^2}\left[\ln\frac{\sqrt{1+\hat{R}_B^2}+1}{2}+\frac{1}{\sqrt{1+\hat{R}_B^2}+1}-\frac{1}{2}\right]+\frac{B}{4}$$

For $\hat{R}_B = 3$, $\hat{z}_H = 1$

$$I_{2c}^{*2} = .635\,A + B = .580 \qquad A = 1.14$$

$$I_{2s2c}^{*2} = .105\,A + .25B = .0832 \qquad B = -.15$$

$$I_{2c}^2 = .747 \qquad I_{2s}^4 = .429$$

$$I_{2c}^3 = .715 \qquad I_{2c}^4 = .697$$

$$I_{2s}^2 = .524 \qquad I_{4c}^2 = .591$$

$$I_{2s}^3 = .464 \qquad I_{2c2s}^2 = .146$$

The effective roll rate is

$$\bar{V}_c\hat{R}_B\, I_{2s}^4 = 1.287\bar{V}_c$$

This can be compared with the value at $\hat{z}_H = 0$ determined from

$$\bar{V}_c \hat{R}_B F_w(\hat{R}_B) = 1.395 \bar{V}_c$$

Varying the size of the helicopter

$$\hat{R}_B = 2 \qquad \hat{R}_B I_{2s}^4 = 1.24$$

$$\hat{R}_B = 1 \qquad \hat{R}_B I_{2s}^4 = .81$$

However it should be noted that $\bar{V}_c \hat{R}_B$ is vortex characteristic divided by Ω so the trend with size given by ratio

$$\frac{I_{2s}^4}{\Omega}$$

and

$$\hat{R}_B = 3 \qquad I_{2s}^4 = .429$$

$$\hat{R}_B^4 = 2 \qquad I_{2s} = .62$$

$$\hat{R}_B = 1 \qquad I_{2s}^4 = .81$$

Ω varies with size due to the fact that helicopters operate at more or less constant tip speed.

The F* values and the first terms in I* are shown in Figure A-3.

It may also be noted from the I integrals that the cos terms are approximately equal to 0.7 v_v while the sin terms are the order of 0.5 v_v indicating that for a rotor radius of $R_B = 3$, the averaged cos effects (which will produce lateral flapping on an articulated rotor) are about 70 percent of the maximum value and the sine effects which will produce longitudinal flapping on an articulated rotor are about 50 percnet of the lateral velocity. These effects were not included in the calculations presented since the longitudinal effects are

small in any case and with the exception of the dihedral effect, the main rotor is only part of the contribution to the other lateral/directional stability derivatives.

TABLE I

HELICOPTER CHARACTERISTICS

UH-1H

	Gross Weight	8000 lbs
Blades = 2	Blade Flapping Inertia	1210.5 slug-ft^2
Rotor Radius = 24 ft	Roll Inertia (I_x)	2925 slug-ft^2
Blade Chord = 1.75 ft	Pitch Inertia (I_y)	10830 slug-ft^2
Hub Type See-Saw	Yaw Inertia (I_z)	9250 slug-ft^2
Rotor RPM 320 RPM	Product of Inertia (I_{xz})	1250 slug-ft^2
Effective Roll Rate 3.23	Rotor Height Above CG	6.58 ft

Bell Bar Feedback Laws:

$$DB + .333\ DB = -4.96\ q$$

$$DA + .333\ DA = 5.95\ p$$

Stability Derivatives (case 140) V_o = 60 kts, W_{RC} = 1200 fpm

	u	w	q	v	p	r	DB	DA
X	-.0255	.0754	1.202	.0065	-1.45	-.369	.883	-.019
Z	.0291	-.866	-1.858	-.0376	-1.884	2.457	2.75	.051
M	.0035	-.0057	- .490	.0012	.199	.0051	- .183	.0016
Y	.0039	-.0172	-1.322	-.131	-1.339	1.651	.0842	.9309
L'	.0005	-.0119	- .830	-.0133	- .799	.325	.0539	.5926
N'	-.0059	-.0016	- .0836	.0348	- .2767	-1.349	.0145	.0832

TABLE I (continued)

Disturbance Terms

	v_v	P_{Ae}
X	-.0065	-1.145
Z	.0376	-1.884
M	-.0012	.199
Y	.131	0
L'	.0133	0
N'	-.0348	- .179*

* Modified to account for inertial effects

Stability Derivatives (case 133) V_o = 100 kts, W_{RC} = 1900 fpm

	u	w	q	v	p	r	DB	DA
X	-.0516	.0853	.8876	.0117	- .945	- .535	.659	- .0229
Z	.109	-.9613	-3.997	-.0481	-3.121	3.071	4.813	.0408
M	.0062	-.0087	- .6133	.0002	.1728	.0419	- .192	.0015
Y	.0088	-.0375	-1.398	-.1897	-1.092	2.213	- .2378	1.019
L'	.0035	-.0227	- .896	-.0145	- .627	.4635	.1411	.647
N'	-.0043	.0071	- .2884	.0434	- .2376	-1.808	- .0323	.0889

TABLE I (Continued)

Disturbance Terms

	v_v	P_{Ae}
X	-.0117	- .946
Z	.048	-3.12
M	0	.1728
Y	.190	0
L'	.0145	0
N'	-.0414	- .162*

*Modified to account for inertial effects.

TABLE I (Continued)

OH-6A

Blades 4		Gross Weight	2550 lbs
Rotor Radius 13.17 ft		Blade Flapping Inertia	46.83 slug-ft^2
Blade Chord .563 ft		Roll Inertia (I_x)	329 slug-ft^2
Hub Type: Articulated with Offset		Pitch Inertia (I_z)	899 slug-ft^2
Hinge Offset .46 ft		Yaw Inertia (I_z)	722 slug-ft^2
Rotor RPM 470 RPM		Product of Inertia (I_{xz})	94.5 slug-ft^2
Effective Roll Rate 6.03		Rotor Height Above CG	3.82 ft

Stability Derivatives (case 25) V_o = 60 kts, W_{Rc} = 1116 Ft/Min

	v	p	r	v_v
Y	-.0906	-1.513	.751	.0906
L'	-.0567	-4.97	-.134	.0567
N'	.0681	- .969	-1.56	-.0681

TABLE I (Continued)

BO-105

Blades 4		Gross Weight	4620 lbs
Rotor Radius 16.11 ft		Blades Flapping Inertia	161.9 slug-ft^2
Blade Chord .886 ft		Roll Inertia (I_x)	1330 slug-ft^2
Hub Type Hingeless		Pitch Inertia (I_y)	3608 slug-ft^2
Flap Frequency Ratio 1.12		Yaw Inertia (I_z)	3266 slug-ft^2
Rotor RPM 430		Product of Inertia (I_{xz})	0
		Rotor Height Above CG	5.16 ft

Stability Derivatives (case 44) V_o = 60 kts, W_{RC} = 1000 fpm)

	v	p	r	v_v
Y	-.088	- 1.88	.56	.099
L'	-.0803	- 9.17	-.0112	.0803
N'	+.0256	-.0758	-.6854	-.0256

Stability Derivatives (case 46) V_o = 100 kts, W_{RC} = 1000 fpm

	v	p	r	v_v
Y	-.133	- 1.57	.81	.133
L'	-.0923	- 8.81	.158	.0923
N'	.0283	-.079	-.843	-.0283

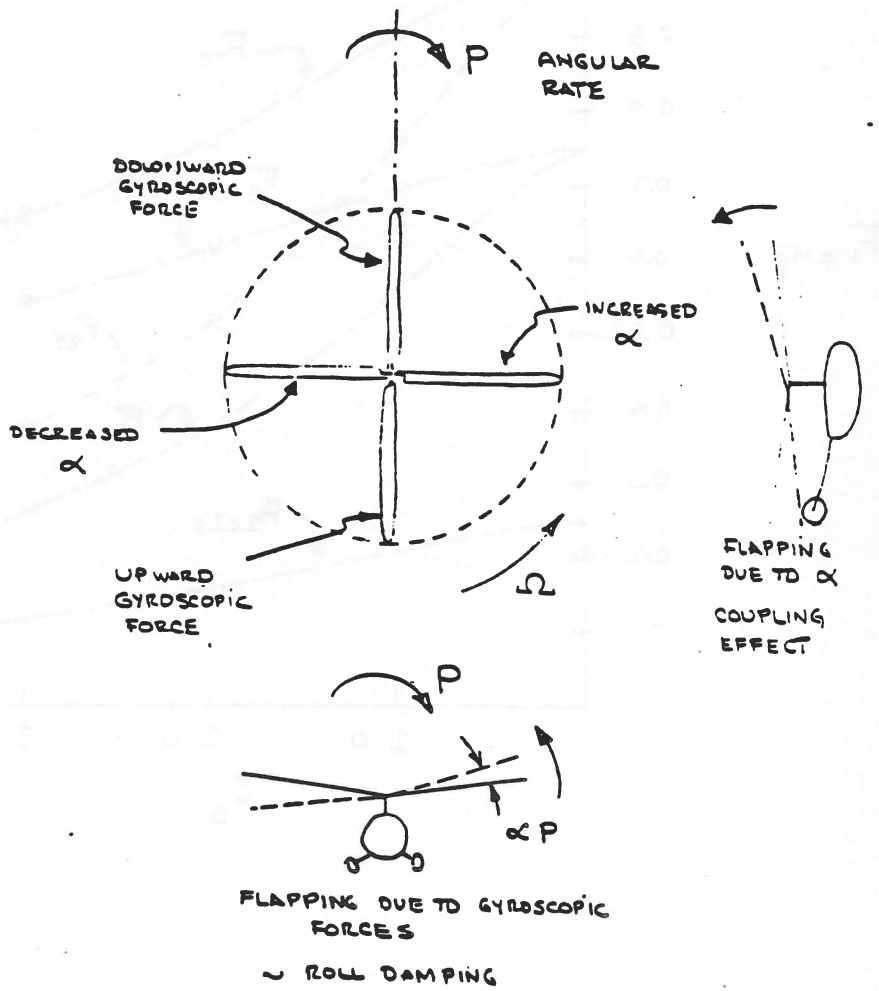

Figure A-1. Shaft Angular Velocity Effects on Rotor Flapping.

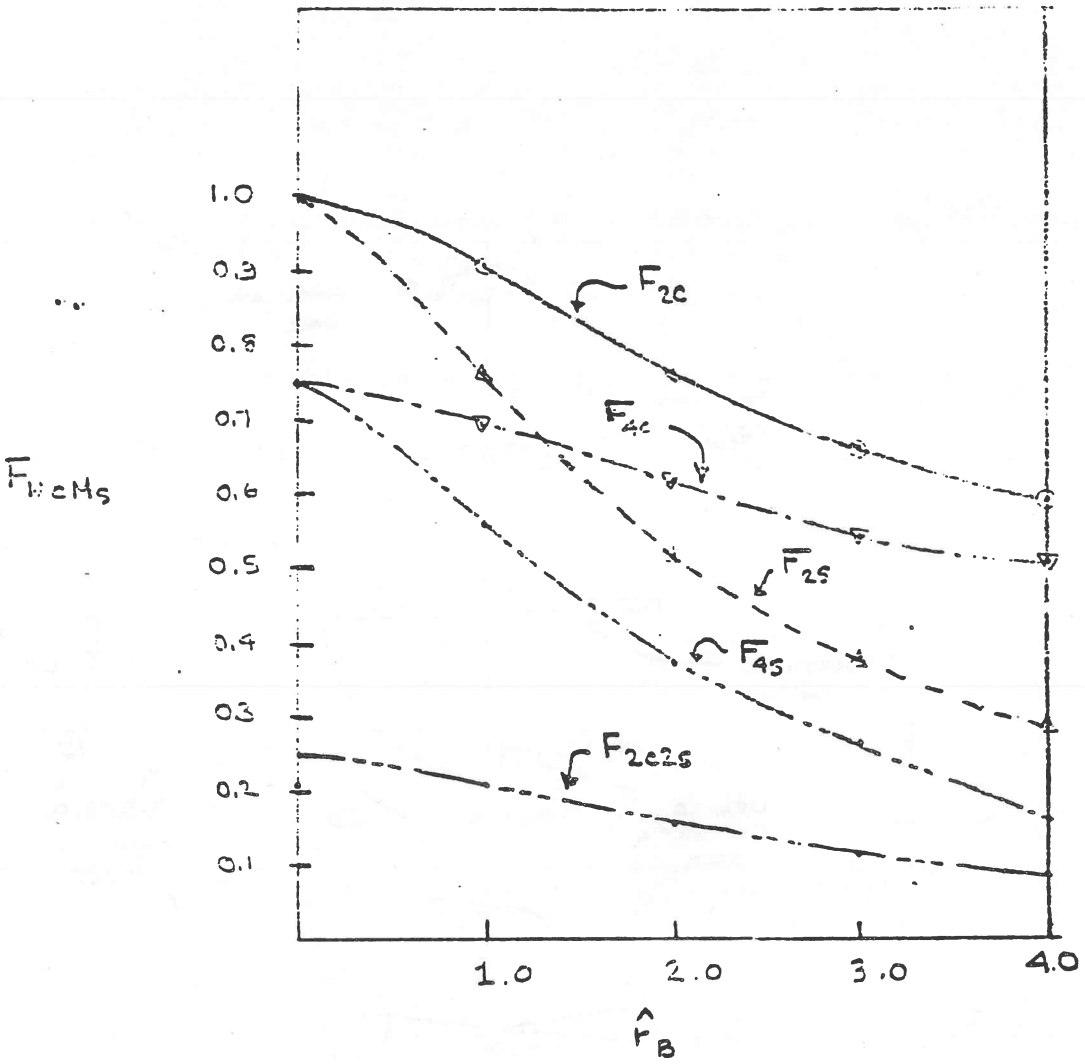

Figure A-2. Values of Integrals for Disturbance Evaluation.

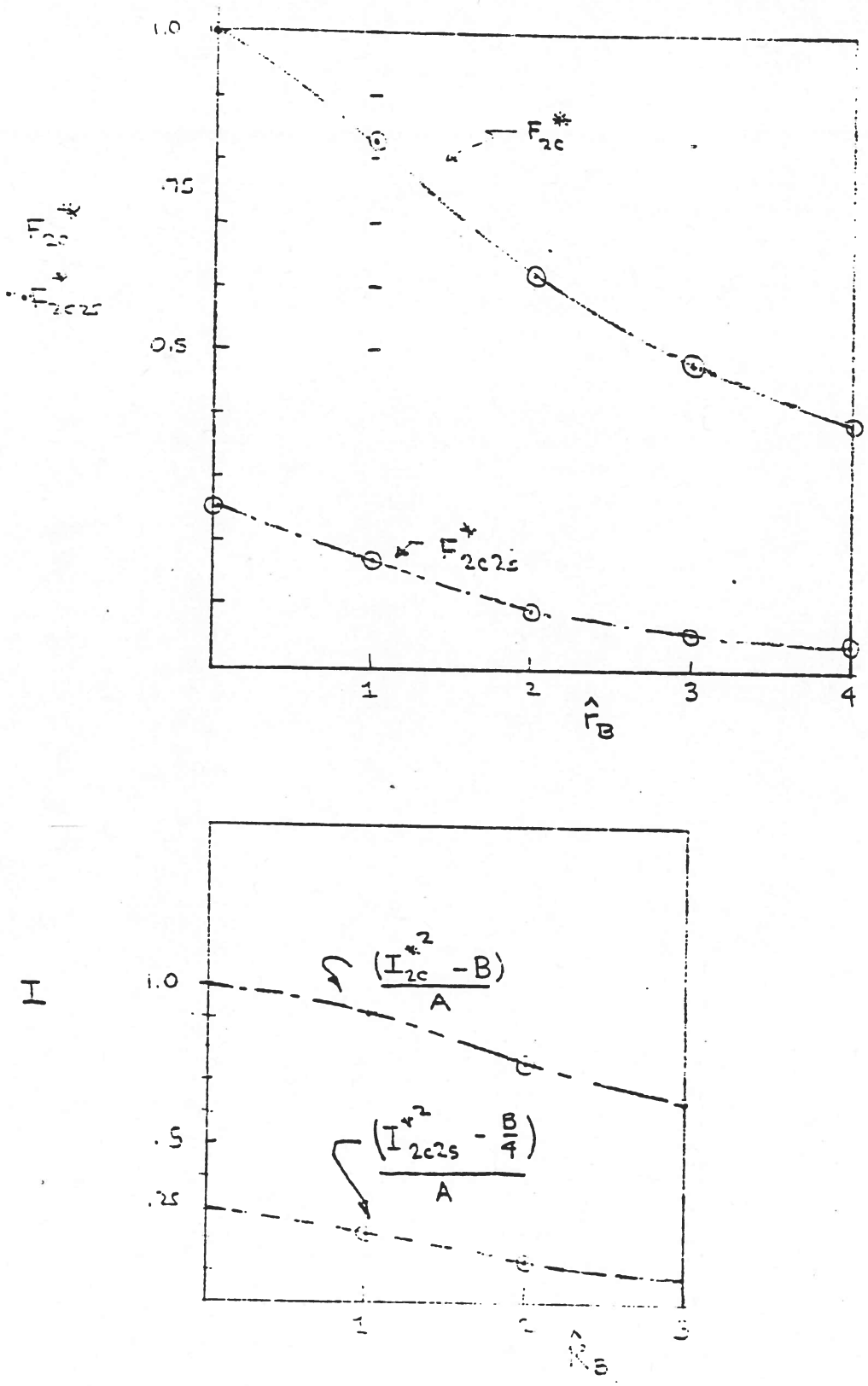

Figure A-3. Values of Integrals for Disturbance Evaluation.